Cell division protein A (CdpA) organises and anchors the division ring at midcell in haloarchaea

Yan Liao[1,#], Vinaya Devidas Shinde[1], Dalong Hu[1,2], Zhuang Xu[3,4], Bill Söderström[1], Katharine A. Michie[5], Iain G. Duggin[1,#]

1. Australian Institute for Microbiology & Infection, University of Technology Sydney, Australia

2. Saw SweeHock School of Public Health, National University of Singapore, Singapore

3. School of Mathematics and Statistics, The University of New South Wales, Australia

5. Structural Biology Facility, Mark Wainwright Analytical Centre, The University of New South Wales, Australia

Current address:

4. Centre for Cancer Genetic Epidemiology, Department of Public Health and Primary Care, University of Cambridge, UK

Address correspondence to Yan Liao (yan.liao@uts.edu.au) and Iain Duggin (iain.duggin@uts.edu.au)

Abstract

Many archaea appear to divide through the coordinated activities of two FtsZ homologues (FtsZ1 and FtsZ2) and another bacterial cell division homologue (SepF), which are part of the midcell division ring. Here, we identify an additional protein (HVO_0739, renamed CdpA) that is involved in cell division in *Haloferax volcanii*, with homologues in other Haloarchaea. CdpA localizes at the mid-cell division ring, and this requires the presence of the ring-assembly protein FtsZ1. The division constriction protein FtsZ2 also influenced the proper midcell assembly and structure of CdpA. In the absence of CdpA, cells frequently failed to divide properly, and FtsZ1 formed poorly condensed pseudo-helical structures spanning across a broad region of the cell, whereas FtsZ2 showed mispositioned foci, nano-rings, and filaments. The rate of directional movement of FtsZ1 and FtsZ2 structures around the division ring appeared minimally affected by loss of CdpA, which resulted in continual repositioning of the aberrant FtsZ structures in the cells. In contrast to the FtsZ proteins, CdpA formed relatively immobile foci around the ring. Protein domain function studies, pull-down assays, and multimer structure predictions suggest that CdpA is part of a membrane complex that tethers FtsZ2 and other division proteins to the midcell membrane. Our discovery of an archaeal FtsZ organisation and midcell anchor protein offers new insights into cell division mechanisms that are similar across the tree of life.

Introduction

Cell division is one of the most fundamental processes in all organisms. It is universally carried out through the localized assembly of cytoskeletal proteins into a ring-like structure linked to the cell membrane and envelope that initiates a constriction process leading to division. In most bacteria, the cytoskeletal protein FtsZ and other cytoskeletal and accessory proteins form the division ring that dynamically drives cell envelope constriction[1]. Bacterial FtsZ appears to perform multiple functions, including acting as scaffolding for protein recruitment to the division site, triggering membrane constriction[2,3], and dynamically guiding cell wall synthesis to drive its inward growth[4,5]. The relative contributions of these mechanisms to division *in vivo* are yet to be precisely defined.

The eukaryotic homolog of FtsZ is tubulin, which greatly elaborates on the core polymerization function common to this superfamily of proteins, and forms microtubules that provide structural support and play essential roles in diverse cellular processes including intracellular transport and division, although tubulin is not considered a main component of the eukaryotic division ring[6,7]. Multiple tubulin proteins exist in each species, with diversified and specialized functions to support the complex cellular events and differentiation processes that they underpin[8].

Most bacterial species contain only one FtsZ, but archaea, which are phylogenetically more closely related to eukaryotes, most commonly have two FtsZ homologues belonging to distinct families[9-11]. The dual-FtsZ system might resemble an early stage in the evolutionary diversification and specialization of cytoskeletal functions, as seen in eukaryotes. By using the archaeal model organism, *Haloferax volcanii*, previous work showed that they divide through the coordinated activities of FtsZ1 and FtsZ2[12,13]. The role of archaeal FtsZ1 was primarily ascribed to promoting assembly of the midcell ring, whereas FtsZ2 was more directly implicated in the ring constriction process[13]. Thus, some of the multiple functions of bacterial FtsZ appear to be at least partially separated into specialized homologs in the archaeal dual-FtsZ system. Furthermore, FtsZ2 was found to be specifically absent in certain methanogenic archaea that—rarely in archaea—have a peptidoglycan (PG) cell wall, suggesting that FtsZ2 is needed for division when a PG wall is not present to support the inward growth of the cell envelope[13].

Current knowledge of FtsZ-based cell division in archaea is limited. There are only a few proteins in this system that have been identified and characterized, despite the many different components present in bacterial and eukaryotic cell division systems. In addition to the two FtsZ proteins, an archaeal homologue of the bacterial division protein SepF[14,15] and the very recently reported PRC barrel domain proteins (CdpB1/2)[16,17] were found to have roles in division. *H. volcanii* SepF associates with FtsZ2 at the division site and potentially the cell membrane[14], and CdpB1 also associates with SepF[16,17]. Crystal structures and AlphaFold2 multimer predictions suggested a tripartite complex formed by CdpB1, CdpB2 and SepF, with CdpB1 and CdpB2 forming a polymer of alternating heterodimers[16]. Currently, there is very little information on what functions these proteins play in the division mechanism or how they are linked to the envelope at midcell.

Other expected components of the FtsZ-based archaeal divisome are yet to be identified, though candidate genes linked to cell division were identified on the basis that their expression or promoter regions were influenced by a transcriptional regulator that appears to control cell division, CdrS, which is encoded by a small ORF in an operon with *ftsZ2*[18,19]. In *H. volcanii*, CdrS-regulated genes included *ftsZ1*, *ftsZ2*, *sepF*, *cdpB1* (Hvo_1691), and the diadenylate cyclase gene (*dacZ*) implicated in signal transduction and regulation of division[19,20]. Another previously uncharacterized gene, HVO_0739, was, with *sepF*, amongst the most strongly regulated by CdrS[19]. Here we have determined the function of HVO_0739, renaming the protein CdpA (Cell division protein A), and we propose the Cdp- prefix may be given to other haloarchaeal proteins when they are discovered to participate directly in the division mechanism. We applied genetic and protein structure-function analyses combined with high-resolution fluorescence microscopy to demonstrate the functions of CdpA in organising the assembly of the two FtsZ proteins to anchor them at midcell for division.

Results

CdpA is conserved in haloarchaea and required for normal cell division in *H. volcanii*

We identified CdpA (HVO_0739) homologs encoded in 506 published archaeal genomes and performed a phylogenetic analysis of the amino acid sequences. The *cdpA* gene is typically present as a single gene in Haloarchaea, in which it co-exists with the two FtsZs (Fig. 1a) in 96.5% of the species analyzed. Based on protein topology and structure predictions (Fig. 1b), and a multiple sequence alignment (Supplementary Fig. 1), CdpA is comprised of three main regions: a conserved N-terminal transmembrane domain, a less conserved cytoplasmic disordered linker region, and a small cytoplasmic C-terminal domain. CdpA does not have a direct homolog in Bacteria or some of the more distantly related archaeal taxa, although we observed homologous CdpA-like proteins, which showed significant homology but differed in length (± 20%) or number of N-terminal transmembrane segments (≠ 4) compared to the reference CdpA (HVO_0739) in a diverse range of archaea (Fig. 1a). Some Halobacteriota species contained multiple homologs within the genome (Fig. 1a). For example, in *H. volcanii*, a CdpA-like protein (HVO_2016) with four predicted transmembrane segments lies adjacent to HVO_2015, which encodes an actin superfamily protein (volactin)[21] hinting of a potential common function associated with diverse cytoskeletal systems.

To identify the role of CdpA, we investigated the consequences of deleting the *cdpA* gene in *H. volcanii*. Microscopy revealed a cell division defect (Fig. 1c), where the Δ*cdpA* mutant showed a mixture of some greatly enlarged cells that had failed to divide and others with almost normal size. This great heterogeneity suggests an incomplete division defect where failure of cell division in some cells leads to enlarged cells that have a lower probability of division than the smaller cells, which further exaggerates their size defect. Consistent with this, time-lapse microscopy of growing Δ*cdpA* cells showed that some divided at mid-cell and others initially developed division planes but were then unable to complete division (Fig. 1d, Supplementary Video 1). Interestingly, some of the greatly enlarged Δ*cdpA* cells appeared to lyse suddenly but produced cell fragments that were sometimes capable of ongoing growth and division (Fig. 1d, arrows; Supplementary Video 1); in others, blebbing from cellular lobes was seen. These appear to be typical features of *H. volcanii* cell division mutants that are accompanied by ongoing chromosome replication and metabolism to maintain culture viability[13].

To verify the cell division phenotype attributed to *cdpA*, we reintroduced the *cdpA* gene under the control of the tryptophan-regulated promoter (*p.tna*) on a plasmid in the Δ*cdpA* background. This rescued the cell division defect in the presence of moderate (0.2 mM) or high (2 mM) concentrations of tryptophan (Trp) (Supplementary Fig. 2), confirming that the *cdpA* open reading frame (ORF) is responsible for the observed cell division phenotype. Overexpression of *cdpA* in a wild-type *H. volcanii* background caused no detected cell division or morphological changes (Supplementary Fig. 2a).

CdpA localizes at the mid-cell division ring

We investigated the subcellular localization of CdpA by expressing GFP-tagged CdpA from a plasmid in wild-type and Δ*cdpA* strain backgrounds. CdpA-GFP fully complemented the cell division defect of the Δ*cdpA* strain in the presence of 0.2 mM Trp induction or greater, showing that the tagged protein is functional in division (Supplementary Fig. 3). Fluorescence microscopy showed that CdpA-GFP in both strains localized as a band at mid-cell in almost all cells (Fig. 1e, Supplementary Fig. 3). With relatively high concentrations of Trp (2 mM), small extracellular fluorescent particles were also seen (Supplementary Fig. 3b), suggesting that excess CdpA-GFP promotes the generation of such particles from cells. Previously, we also detected comparable small extracellular fluorescent particles detached from cells with minimal division defects when expressing mCherry-tagged FtsZ1 GTPase mutant in a wild-type *H. volcanii* strain[13]. However, the mechanisms underlying the formation of these extracellular fluorescent particles remain unclear. One possible explanation is a budding-like process, as previously observed in *ftsZ* knockout strains[13].

139 We then investigated the localization of CdpA together with FtsZ1 or FtsZ2 by production of pairs of
140 fusion proteins from a plasmid in the wild-type background. The degree of co-localization observed
141 between CdpA-GFP and FtsZ1-mCherry was strong, with a correlation coefficient of > 0.7 in 79% of
142 cells (Fig. 2a). CdpA-GFP showed a somewhat higher background throughout the rest of the cell than
143 FtsZ1-mCherry, relative to the midcell bands (Fig. 2a, normalized intensity graphs). The co-production
144 of CdpA-GFP and FtsZ1-mCherry did not cause a substantial change in cell shape and size, similar to
145 when FtsZ1-mCherry or FtsZ2-mCherry are moderately produced[13]. The co-production of CdpA-GFP
146 and FtsZ2-mCherry resulted in enlarged or filamentous cells (Fig. 2a), suggestive of a functional
147 interference between these two tagged proteins. Nevertheless, CdpA-GFP and FtsZ2-mCherry still
148 showed strong co-localization, with 84% of cells having a correlation coefficient of > 0.8 (Fig. 2a,
149 righthand panels). In many of these enlarged cells, CdpA-GFP and FtsZ2-mCherry were co-localized
150 around mid-cell, whereas in some cells they were found near the quarter positions of the long axis of
151 the cell (Fig. 2a).

152 We next investigated whether CdpA-FtsZ co-localization depends on the presence of the other FtsZ
153 protein (Supplementary Fig. 4). In the absence of FtsZ1, FtsZ2-mCherry formed patches or foci, with
154 CdpA-GFP co-localizing well with these structures. However, CdpA-GFP also appeared as faint,
155 discontinuous foci along the cell edge or as short patches inside the cells, where FtsZ2-mCherry was
156 not present. In the absence of FtsZ2, CdpA-GFP and FtsZ1-mCherry appeared as broader bands,
157 perpendicular patches or foci, exhibiting substantial co-localization, with some minor regions of weak
158 localization of CdpA-GFP only. The above findings suggest that CdpA has a significant role in organising
159 the assembly of the two FtsZ proteins at the midcell ring.

160 **CdpA, FtsZ1 and FtsZ2 do not strongly colocalize within the division ring**

161 To investigate protein localization at higher resolution within the division ring, Structured-Illumination
162 Microscopy (SIM) was used to visualize cells co-producing CdpA- and FtsZ- fusion proteins. Live cell
163 2D-SIM revealed that CdpA-GFP and FtsZ1/2-mCherry showed different patterns of fluorescence
164 within the mid-cell ring (Fig. 2b). Specifically, quantification of fluorescence intensities revealed that
165 CdpA-GFP and FtsZ1- or FtsZ2-mCherry foci were colocalized in some regions but were clearly
166 separated in others (Fig. 2b). Similarly, FtsZ1-mCherry and FtsZ2-GFP exhibited only partial co-
167 localization within the mid-cell ring, as revealed by 2D-SIM (Supplementary Fig. 5).

168 We then used 3D-SIM, which further resolved the individual ring sub-structures. CdpA-GFP was highly
169 discontinuous within the ring, appearing as distinct small foci with gaps in fluorescence intensity
170 between them (Fig. 2c). FtsZ1-GFP and FtsZ2-GFP rings appeared more continuous but still showed
171 substantial variations in structure and intensity around the ring (Fig. 2c, Supplementary Fig. 6,
172 Supplementary Video 2-4).

173 **CdpA requires FtsZ1 and FtsZ2 for its proper assembly at midcell**

174 The division ring localization of CdpA, FtsZ1 and FtsZ2, and their different spatial patterns within the
175 ring, prompted us to investigate the dependency of CdpA and FtsZ1/FtsZ2 on each other for proper
176 assembly in the division ring. We assessed the localization of CdpA in the two *ftsZ* knockout strains
177 and vice versa. In the absence of FtsZ1, CdpA-GFP failed to localize as rings and infrequently appeared
178 as a faint midcell focus, and in an *ftsZ1/ftsZ2* double knock-out it showed a diffuse, non-localized signal
179 (Fig. 3a). On the other hand, FtsZ2 deletion did not prevent CdpA-GFP localization although it often
180 appeared as very irregularly structured, poorly condensed or indistinct rings (Fig. 3a). Thus, the proper
181 localization and midcell assembly of CdpA is strongly dependent on the presence of FtsZ1 and FtsZ2.

182 **CdpA organizes FtsZ1 and FtsZ2 filaments for proper midcell ring formation**

183 Deletion of *cdpA* had strikingly different effects on FtsZ1 and FtsZ2 function and localization patterns.
184 FtsZ1-mCherry localizations in Δ*cdpA* appeared as rings but with broader zones compared to FtsZ1-
185 mCherry ring structure in wild-type cells and occasional foci seen throughout the cells (Fig. 3b).

186 Measurements of the ratio of localized to non-localized FtsZ1-mCherry per cell and each individual
187 localization's thickness (or its width along the medial axis), confirmed that the fluorescence in localized
188 structures was similar in both strains, but the localizations were relatively poorly condensed in many
189 of the *ΔcdpA* cells compared to wild-type (Fig. 3b, graphs). In these strains, the *cdpA* knockout resulted
190 in ~30% of the total cells that we classified as filamentous (cell area > 5 μm^2, circularity < 0.3) compared
191 with ~5% in the wild-type (Supplementary Fig. 7). These findings suggest that CdpA contributes to
192 proper FtsZ1 ring condensation.

193 Consistent with a previous observation[13], we saw that production of FtsZ2-GFP caused a division
194 defect in the wild-type background, resulting in somewhat enlarged cells and some showing multiple
195 rings (Fig. 3c). However, in the Δc*dpA* background, FtsZ2-GFP showed fewer rings of normal
196 appearance, and instead frequently assembled as foci, clusters of multiple foci, or short mispositioned
197 filaments located along the cell edge in a perpendicular orientation compared to normal rings (Fig. 3c).
198 Automated detection of the frequency of FtsZ2-GFP rings along the cell length confirmed that there
199 were overall fewer rings in the Δc*dpA* background compared to the wild-type (Fig 3c - compare the
200 number of cells in each group sorted by the number of detected rings). We also observed similar
201 mispositioned or perpendicular structures of FtsZ2-mCherry in the absence of CdpA (Supplementary
202 Fig. 8). These observations suggest that a key role of CdpA is the organisation of FtsZ2 filaments into
203 properly structured and orientated rings.

204 Highly informative results were obtained when producing both FtsZ1-mCherry and FtsZ2-GFP in the
205 Δ*cdpA* background. The absence of CdpA resulted in obvious uncoupling of FtsZ1-mCherry and FtsZ2-
206 GFP filaments, with a wide range of correlation coefficients (0.3-1) in most cells (Fig. 3d). FtsZ1-
207 mCherry appeared as rings with additional poorly condensed foci throughout the cells, whilst FtsZ2-
208 GFP was seen as foci or mispositioned filaments, as seen during the single expression experiments
209 above (Fig. 3d). Experiments with a lower concentration of tryptophan inducer (0.1 mM Trp), to reduce
210 the concentration of FtsZ1-mCherry and FtsZ2-GFP[13], still showed similar patterns with broad zones
211 of FtsZ1-mCherry localization and foci or mispositioned FtsZ2-GFP (Supplementary Fig. 9).

212 We used 3D-SIM to further investigate the unusual FtsZ2-GFP patterns in the absence of CdpA. FtsZ2-
213 GFP bands observed in widefield images were seen as incomplete and poorly organized rings in 3D-
214 SIM (Supplementary Fig. 10-11). Furthermore, some of the FtsZ2-GFP foci in widefield were resolved
215 as nano-rings, -helices, or short filaments in 3D-SIM (Supplementary Fig. 10-11, Supplementary Video
216 5), which were not associated with division constriction sites. The FtsZ2-GFP nano-rings displayed
217 variation in orientation and size, ranging approximately from 300 to 700 nm (mean ± SEM = 463 ± 18
218 nm, n = 40). Additionally, the perpendicular filaments of FtsZ2-GFP apparent in widefield images were
219 clearly resolved as mostly straight filaments along the cell edge in 3D-SIM (Supplementary Fig. 10-11).

220 We conclude that CdpA plays an important role in organization of FtsZ1 and FtsZ2 at midcell by
221 promoting FtsZ1 ring condensation and the correct organization, orientation and assembly of FtsZ2
222 filaments.

223 **CdpA is a relatively immobile midcell ring 'anchor' that has minimal effects on the dynamics of FtsZ1-**
224 **GFP and FtsZ2-GFP assemblies**

225 To investigate CdpA and FtsZ movement at midcell, and whether CdpA influences FtsZ dynamics within
226 the division ring, we monitored the fluorescence of CdpA-GFP and FtsZ1/2-GFP in live cells over time.
227 We initially recorded 3D-SIM images with 1 min intervals and saw that FtsZ1-GFP was dynamic within
228 the ring, with changes in the intensity and location of clusters of fluorescence intensity over time
229 (Supplementary Fig. 12, Supplementary Video 6), consistent with previous lower-resolution
230 observations[13]. In contrast, CdpA-GFP showed no such movement in the ring over the same period
231 (Supplementary Fig. 13, Supplementary Video 7).

232 To better enable cluster tracking and reduce bleaching during image acquisition, we used total internal
233 reflection fluorescence (TIRF) microscopy to record protein movement near the cell surface closest to
234 the coverslip. Visual inspection of kymographs generated from the TIRF data recorded at the division
235 ring using 4 s frame intervals over 15 min, suggested that clusters of FtsZ1-GFP fluorescence were
236 moving in a directional manner (Fig. 4a). Further analysis revealed that these clusters exhibited
237 complex zigzag and crossover patterns, reflecting FtsZ1-GFP cluster movement in both directions
238 around the division plane (Fig. 4a, Supplementary Video 8-9). FtsZ2-GFP showed similar zigzag-like
239 patterns, but they were generally slower than FtsZ1-GFP (imaging required 10 s intervals over 40 min,
240 Fig. 4b, Supplementary Fig. 14, Supplementary Video 10-11). In contrast, visualization of CdpA-GFP
241 with TIRF over the 15- and 40-min periods showed no substantial directional movement and greatly
242 reduced fluctuations of fluorescence intensity over time compared to the FtsZs (Fig. 4c, 4d,
243 Supplementary Fig. 14-15, Supplementary Video 12-15).

244 It is important to note that the function of FtsZ2-GFP in cell division is more severely affected by the
245 GFP tag than FtsZ1-GFP[13,22], whereas CdpA-GFP is fully functional (Fig. 1f). The dynamics of FtsZ2-GFP
246 or its response to other proteins might therefore be significantly affected by the tag, compared to the
247 untagged native FtsZ2. Here, our main aim was to determine whether the relative dynamics of each
248 of the existing FtsZ-GFPs is altered by the presence or absence of CdpA. In the absence of CdpA, FtsZ1-
249 GFP still showed clusters with apparently similar movement rates as the wild-type background, and as
250 expected, they often spanned a relatively uncondensed zone around midcell (Fig. 4e, Supplementary
251 Video 16-18). We then measured the FtsZ1-GFP fluorescence intensity over time in a square region
252 near the centre of a localization, and this appeared to show irregular, non-periodic fluctuations (Fig.
253 4f, Supplementary Fig. 16). To identify any periodicity or dominant frequencies, we plotted the power
254 spectrum density (PSD)[5] in 21 cells of each strain (Fig. 4g, Supplementary Fig. 17). In the wild-type
255 background, there was an elevated FtsZ1-GFP periodicity at ~0.003 Hz on average compared to Δ*cdpA*
256 in which the average fluctuations showed a simpler decay-like curve consistent with a lack of
257 periodicity detected within the 15 min. The wild-type signal around 0.003 Hz was dominant in ~24%
258 of cells, and weak or not evident in ~76%. This heterogeneity might reflect complex patterns of
259 polymerization within the ring, or cells at different stages of midcell maturation and activity
260 (Supplementary Fig. 17). In the absence of CdpA, FtsZ1 polymerization rates or types might be affected,
261 or the loss of ring structural integrity could also lead to the loss of the localized periodic fluctuations.

262 With FtsZ2-GFP in Δ*cdpA*, we saw striking dynamic shifts in the cellular position and orientation of
263 FtsZ2-GFP structures over time (Fig. 4h-i, Supplementary Video 19-24), consistent with the strong
264 uncoupling and mispositioning of FtsZ2-GFP seen in the static images (Fig. 3c). However, like FtsZ1-
265 GFP, FtsZ2-GFP clusters clearly displayed movement consistent with dynamic polymerization within
266 the localized structures in Δ*cdpA* that was comparable to the wild-type background (Fig. 4h-i,
267 Supplementary Video 10-11, 19-24). We conclude that CdpA is relatively immobile within the ring but
268 strongly influences the stable organization and positioning of the two FtsZ proteins at midcell whilst
269 having minimal or moderate influence on FtsZ-GFP assembly dynamics.

270 **The three domains of CdpA make different contributions towards its function**

271 CdpA contains a strongly predicted N-terminal transmembrane domain (amino acids 17-149), a
272 cytoplasmic unstructured linker region (150-284) and a smaller C-terminal domain (285-328) (Fig. 1b,
273 5a). Together with the results above, this expected topology suggests a model in which CdpA tethers
274 and/or helps assemble and orientate cytoplasmic FtsZ filaments and potentially other components at
275 the midcell membrane. We further investigated this by assessing the contributions of the three main
276 regions to CdpA localization and function.

277 We initially found that an isolated N-terminal domain ($CdpA_{NTD}$-GFP) localized weakly at mid-cell, a
278 NTD deletion construct ($CdpA_{\Delta NTD}$-GFP) failed to localize, and a CTD deletion construct ($CdpA_{\Delta CTD}$-GFP)
279 efficiently localized at mid-cell (Fig. 5b). The $CdpA_{NTD}$ is therefore essential for midcell ring localization,

280 but insufficient without the $CdpA_{Linker}$ for the normal degree of localization. It is possible that the linker
281 contributes to interactions promoting CdpA's assembly into the ring, and/or it alleviates potential
282 steric interference by the GFP when attached directly to the $CdpA_{NTD}$.

283 To investigate the influence of the three CdpA domains on cell division and FtsZ localization, we
284 generated in-frame deletions (scar-less) of each of the three regions in the endogenous chromosomal
285 copy of *cdpA*. In the absence of the NTD (*cdpA*$_{\Delta NTD}$), the cells became filamentous (Fig. 5c,
286 Supplementary Fig. 18a); the *cdpA*$_{\Delta Linker}$ strain also showed a division defect of enlarged plate cells,
287 and *cdpA*$_{\Delta CTD}$ showed a heterogeneous mixture of enlarged plates and filamentous cells. Thus, division
288 defects were clear in all three strains, but they have different cell morphologies. However, these shape
289 differences were neutralized upon transformation with plasmids (containing various FtsZ-FPs), which
290 resulted in a greater frequency of highly filamentous cells (circularity < 0.2) and no enlarged plates
291 (Fig. 5c, Supplementary Fig. 18a). This is consistent with the known influence of *H. volcanii* plasmids
292 on cell shapes[22].

293 In all three CdpA domain deletion backgrounds, FtsZ1-mCherry appeared as poorly condensed rings,
294 broad zones of patchy localization or complex helicoid structures, but this was accentuated with
295 *cdpA*$_{\Delta Linker}$ (Fig. 5c, Supplementary Fig. 18b), suggesting that this deletion causes additional
296 interference to FtsZ1 localization. Cells producing FtsZ2-GFP in all three domain deletion backgrounds
297 were filamentous, with infrequent rings or localizations usually near one or both poles (Fig. 5c). In the
298 *cdpA*$_{\Delta Linker}$ background, rings were very rare and foci were frequently seen near the pole, suggesting
299 this deletion results in additional interference to prevent normal FtsZ2-GFP assembly. In contrast, the
300 *cdpA*$_{\Delta CTD}$ background gave the mildest FtsZ2-GFP assembly defects, with rings appearing more
301 frequently than in other mutants, although still less frequently than in the wild-type (Fig. 5c,
302 Supplementary Fig. 18c). Additionally, mispositioned or perpendicular structures of FtsZ2-GFP were
303 also evident in three domain deletion strains (Supplementary Fig. 19).

304 When we co-produced FtsZ1-mCherry and FtsZ2-GFP in the three domain deletion strains (Fig. 5d,
305 Supplementary Fig. 20), the patterns for each protein were similar but some appeared more
306 accentuated than the corresponding single-FtsZ-FP strains. In the *cdpA*$_{\Delta NTD}$ strain, FtsZ1-mCherry
307 localized as rings, poorly condensed rings or foci, while FtsZ2-GFP formed patches, foci, or rare poor
308 rings and they showed a weaker correlation of localization than the wild-type (Fig. 5e). In the *cdpA*$_{\Delta Linker}$
309 strain, FtsZ1-mCherry showed striking irregular bands scattered along the length of the cells, and
310 FtsZ2-GFP showed a combination of diffuse signal with additional scattered foci (Fig. 5d). This strain
311 showed the weakest co-localization amongst the three *cdpA* domain deletions (Fig. 5e) and the FtsZ1-
312 mCherry localizations also occupied a much greater area of the cells than the FtsZ2-GFP localizations
313 (Fig. 5f). In *cdpA*$_{\Delta CTD}$, we saw strongly co-localized rings of FtsZ1-mCherry and FtsZ2-GFP, but these still
314 appeared less frequently than in the wild type and were often near one pole (Fig. 5d-f).

315 The combined results suggest that: 1) The N-terminal transmembrane domain and possibly the linker
316 region of CdpA are important for CdpA midcell localization, FtsZ1 ring condensation, and FtsZ2 ring
317 assembly and positioning; 2) The linker region of CdpA is necessary to prevent strong localization
318 defects caused by direct fusion of the NTD and CTD, possibly by preventing steric hindrance; 3) The C-
319 terminal domain of CdpA does not play a major role in the assembly and coupling of FtsZ1 and FtsZ2
320 rings, but has at least one other significant yet currently unknown role in cell division.

321 **CdpA is part of an anchor complex linked to FtsZ2 and other cell division proteins**

322 The SepF division protein *in H. volcanii* has been shown to interact directly or indirectly with FtsZ2 and
323 was suggested to be a membrane anchoring protein for FtsZ2[14]. So we investigated the effects of CdpA
324 absence on SepF localization, and vice versa. In the absence of CdpA, SepF-GFP expressed at moderate
325 levels (0.2 mM Trp) formed sharp midcell bands in the small plate cells, and in giant plate-like cells it
326 appeared as complex clusters that appeared detached from the envelope—similar to the patterns
327 observed for FtsZ1/2 in giant plate cells (Supplementary Fig. 21)[13]. However, higher expression of

328 SepF-GFP (2 mM Trp) resulted in the formation of striking branched and less condensed mid-cell bands
329 in the small plate cells (Fig. 6). Conversely, during SepF depletion (as SepF could not be deleted[14]),
330 CdpA-GFP formed very few rings, which were consistently positioned approximately one wild-type cell
331 length from the poles of the highly filamentous cells (Fig. 6b). Plotting the number of CdpA-GFP rings
332 over the cell length in the cell population confirmed that ring frequency along the cells was much
333 lower than in the wild-type background (Fig. 6b). These findings suggest that correct CdpA assembly
334 depends on SepF, while SepF localization is, in turn, influenced by the presence of CdpA.

335 Given the pronounced abnormalities in SepF-GFP localization at higher expression levels in the
336 absence of CdpA, we further examined how the three domains of CdpA influence SepF-GFP
337 localization under these conditions. In the three CdpA domain mutants, SepF expression failed to fully
338 complement the cell division defects, leading to the formation of giant, filamentous cells
339 (Supplementary Fig. 21). In $cdpA_{\Delta NTD}$, SepF-GFP structure at midcell significantly disrupted, forming
340 branched bands, whereas in $cdpA_{\Delta CTD}$ and $cdpA_{\Delta linker,}$ SepF-GFP localizations remained largely
341 unaffected (Fig. 6). These findings suggest that the N-terminal domain (NTD) of CdpA plays a more
342 direct role in mediating SepF assembly at midcell.

343 Given the above results, we searched for CdpA interactions with other *H. volcanii* proteins by isolating
344 affinity-tagged CdpA (CdpA-HA) from cross-linked *H. volcanii* whole-cell lysates. Proteins remaining
345 bound to the anti-HA magnetic beads after washing with a mild-detergent buffer to reduce non-
346 specific associations were eluted and analysed by western blots probed with antibodies recognising
347 HA, FtsZ1 and FtsZ2 (Fig. 7a). Both FtsZ1 and FtsZ2 were detected in the lysate (L) and unbound (FT)
348 samples, but only FtsZ2 was clearly detected in the bound protein elution (E) sample (Fig. 7a). Neither
349 protein was detected in the elution from the control cells containing the HA vector only (Fig. 7a). These
350 results suggest that CdpA can exist in a complex with FtsZ2.

351 We carried out additional pull-down experiments with CdpA-HA and FtsZ2-HA in their corresponding
352 knock-out backgrounds, compared to the wildtype background with HA vector only as the control, and
353 identified bound proteins by mass spectrometry (MS) (Supplementary Table 3). FtsZ1 was detected in
354 the bound-protein elution of both the CdpA-HA and FtsZ2-HA pull-downs, albeit with only moderate
355 statistical support, as assessed by mean MS peak area quantification (Log_2 fold-change (FC)=2.7,
356 p=0.10 for the CdpA-HA pull-down, and Log_2FC=3.0, p=0.03 for the FtsZ2-HA pull-down, n=6
357 independent experiments each). FtsZ2 was identified significantly in the CdpA-HA pulldown
358 (Log_2FC=5.7, p=0.002), and as expected in the FtsZ2-HA pull-down (Log_2FC=10.6, p=0.08). The FtsZ2-
359 HA pull-down only identified one other protein with statistical support (i.e., CetZ2, which was not
360 detected in the HA controls; Supplementary Table 3). The low detection rate in the FtsZ2-HA pull-
361 downs might be due to the relatively low production of the FtsZ2-HA fusion (Supplementary Fig. 22),
362 interference by the HA tag (as seen with the function of FtsZ2-GFP) or possibly limited stability of
363 FtsZ2-HA protein complexes in this assay. However, the CdpA-HA construct was produced and
364 complemented the division defect of the Δ*cdpA* background used in the pull-downs (Supplementary
365 Fig. 22). The CdpA-HA pull-down MS data included other proteins previously implicated in cell division,
366 including SepF (HVO_0392, Log_2FC=4.3, p=0.01), CdpB1 (HVO_1691, Log_2FC=3.4, p=0.07) and CdpB2
367 (HVO_1964, Log_2FC=3.1, p=0.02) (Supplementary Table 3). Other identified proteins recently linked to
368 cell envelope-related functions included actin-like protein volactin (HVO_2015, Log_2FC=2.5, p=0.06)
369 and small GTPase ArvA (OapA, HVO_3014, Log_2FC=2.8, p=0.04)[21,23]. It is currently unknown whether
370 these represent direct or indirect associations with CdpA.

371 To predict how the cell division proteins interact with CdpA, we used Alphafold2 (AF2) Multimer with
372 two molecules each of CdpA, CdpB1, CdpB2, FtsZ2, and SepF, as preliminary AF2 runs and existing
373 homolog structures[16,17] had indicated that each protein can dimerise or polymerise. This revealed a
374 strikingly coherent predicted structure, consistent with the current experimental results, that we refer
375 to as the anchor complex (Fig. 7b). Most of the visible interactions within the predicted anchor
376 complex are supported by low pairwise alignment error scores between the corresponding regions

377 (Fig. 7c). The main exception to these relatively strong predictions was that the association between
378 the anchor complex and FtsZ2 was quite weak, hinting that interactions between the anchor complex
379 and FtsZ2 might occur via other unknown adaptors. The strongly predicted interactions notably
380 include a direct association of the cytoplasmic short N-terminal helix of CdpA (residues 1-10) with the
381 interface region of each CdpB1/2 heterodimer, which would bring CdpB1/2 close to the inner surface
382 of the membrane (Fig. 7b, 7c). Furthermore, CdpA is predicted to participate in a ternary association
383 with CdpB1 and SepF's N-terminal extension and membrane targeting sequence (MTS) that places the
384 SepF MTS in an ideal position to penetrate the inner leaflet of the cytoplasmic membrane whilst also
385 bound to CdpA at the interface of cytoplasm and membrane (Fig. 7b, 7c).

386 These experimental results and structural analysis have indicated that the CdpA NTD acts as a primary
387 membrane anchor located at discrete positions around the division ring, where SepF is expected to
388 play an adaptor-like role (braced by CdpB1/2 multimers) to connect the anchor complex with
389 cytoplasmic ring components including FtsZ2. We found that CdpA has multiple functions, as the inter-
390 domain disordered linker was critical for the proper condensation and positioning of FtsZ1 and FtsZ2
391 filaments, respectively, whereas the CTD was also important for division in other ways, likely through
392 unknown interaction partners.

393

394 **Discussion**

395 In bacteria and eukaryotes, many proteins have been identified to contribute to division ring assembly
396 and anchoring. Here we identify and characterize the function of a ring assembly and anchor protein
397 in haloarchaea, which we named Cell division protein A (CdpA). We found clear roles for CdpA in
398 orchestrating the midcell assembly and co-positioning of FtsZ1 and FtsZ2 filaments to form the division
399 ring in the model archaeon *H. volcanii*. Several other proteins involved in archaeal dual-FtsZ division
400 have recently been identified, including SepF, CdpB1, and CdpB2[14,16,17], though their functions in the
401 haloarchaeal division mechanism are unclear. Based on the current findings, we developed a structural
402 model in which CdpA acts as the membrane-embedded component of a midcell anchor complex
403 (including SepF, CdpB1, and CdpB2 linked to the membrane though multiple direct interactions with
404 CdpA; Fig. 7). CdpA also functions as a tether and organizing center at relatively immobile and distinct
405 locations around the division ring to promote FtsZ1 and FtsZ2 ring formation and maintenance, and
406 likely other midcell ring proteins, via its cytoplasmic linker and C-terminal domains.

407 In bacteria, one of the best characterized FtsZ membrane linkage proteins is the widespread FtsA
408 actin-superfamily protein. The essentiality of FtsA varies among different species. For example, in
409 *Escherichia coli*, FtsA is essential[24], whereas in *Bacillus subtilis*, the *ftsA* gene can be deleted, although
410 this affects Z-ring formation and causes cells to become enlongated[25]. Here, we were able to delete
411 the *cdpA* gene in *H. volcanii*, which caused a division defect resulting in mixed populations of near-
412 normal and greatly enlarged cells. We directly observed some of the greatly enlarged cells forming
413 cellular fragments upon lysis of the main cell body, some of which were viable and capable of ongoing
414 growth and division. This likely explains the survival of many *H. volcanii* cell division mutant strains in
415 culture. Additionally, the *cdpA* deletion strain might survive through the activity of other division site
416 stabilizing or anchoring proteins like SepF[14,26] or CdpB1/2[16,17] that potentially compensate for the loss
417 of CdpA. Other currently uncharacterized haloarchaeal proteins, potentially including CdpA-like
418 proteins, may also be involved in midcell ring assembly or cytoskeletal protein anchoring, helping
419 compensate for the loss of CdpA.

420 Super-resolution imaging revealed that CdpA forms a more discontinuous or patchy ring-like structure
421 at mid-cell compared to FtsZ1 or FtsZ2 rings and differing organization within the ring. In absence of
422 CdpA, FtsZ1 rarely formed normal Z rings and instead formed broad and ill-defined—often helicoid—
423 structures, that still retained dynamic localization patterns. Although typical-looking FtsZ2-GFP rings
424 were sometimes observed in the absence of CdpA, FtsZ2-GFP foci or filaments frequently appeared
425 strongly mispositioned, including perpendicular to the normal ring along the cell edge. FtsZ2 also
426 retained its dynamic properties, resulting in frequent repositioning of the misplaced FtsZ2 foci and
427 filaments. This resulted in FtsZ1 and FtsZ2 becoming uncoupled in their subcellular localization
428 patterns, supporting the notion that they can polymerize independently of one another[13].

429 Our protein pull-down experiments detected CdpA in complex with FtsZ2 but not clearly with FtsZ1,
430 despite our finding that the proper localization of CdpA depends on the presence of both FtsZ2 and
431 especially FtsZ1 (and vice versa). Current observations would suggest that FtsZ1 associates only
432 indirectly with the CdpA-anchor complex, via another anchor, or in a manner that is not well
433 maintained during the pull-down assay procedure. The CdpA-HA pull-down assays also identified SepF
434 and CdpB1/2 amongst the interaction partners. Consistent with this, we found that SepF contributes
435 to CdpA assembly at midcell, and thatSepF's proper localization is strongly affected by the absence of
436 CdpA. Furthermore, the co-localization of CdpA with each FtsZ in strains lacking the other FtsZ suggests
437 a functional interdependence between CdpA and the two FtsZ proteins. Together with the
438 observations of similar poorly-condensed Z-ring structures in the absence of CdpA, SepF[14], or

439 CdpB1/2[16,17], the combined results support a model in which these proteins assemble into a complex
440 that functions in Z-ring assembly.

441 Previous studies reported that *H. volcanii* SepF is part of a complex with FtsZ2[14], and with CdpB1/2[16,17].
442 Furthermore, SepF appears to localize at mid-cell via a short N-terminal amphipathic sequence, which
443 was expected to act as a membrane targeting sequence (MTS)[14]. The finding that the SepF MTS alone
444 was sufficient for midcell ring localization[14] suggests that this short sequence does more than just
445 potential membrane targeting. Additionally, our data indicate that N-terminal domain of CdpA plays
446 a more direct role in mediating interactions with SepF (Fig. 6). Our combined results and structural
447 modelling (Fig. 7) support the existence of a midcell anchor complex that forms through multiple
448 intimate associations, including the N-terminal extensions of CdpA and SepF interacting in different
449 ways with CdpB1/2 heterodimers, and SepF's MTS (at the very N-terminus) simultaneously associating
450 with the CdpA NTD and partly embedded in the cytoplasmic membrane. The SepF MTS may thereby
451 be sufficient for midcell localization[14] due to its likely association with CdpA. The main membrane
452 anchoring component appears to be the CdpA NTD, linked to and braced by multimers of SepF and
453 CdpB1/2.

454 Consistent with the structural model (Fig. 7), our domain localization studies indicated that the CdpA
455 NTD is essential for its midcell localization, whereas the CTD was dispensable for midcell localization
456 but required for normal division. The NTD and linker regions appear to be critical for assembly and
457 anchoring of FtsZ1 and FtsZ2 rings, whereas the CTD seems to not strongly affect FtsZ1 and FtsZ2.
458 These observations suggest a multi-functional role of CdpA in *H. volcanii* division, where the long,
459 disordered linker and C-terminal domain also play important but currently undefined roles in tethering
460 or assembling other proteins at midcell.

461 CdpA shows some noteworthy similarities and differences to other division ring anchor proteins. In
462 bacteria, the FtsZ ring is typically anchored to the midcell membrane by FtsA, ZipA or SepF, whereas
463 in non-FtsZ archaeal division, based on the ESCRT-III (CdvB) cytoskeletal proteins, CdvA is considered
464 to play a different anchor-like role. FtsA is broadly conserved in most bacteria and contains a short C-
465 terminal MTS and also directly interacts with FtsZ, recruiting it to the inner membrane[27,28]. ZipA is an
466 integral inner membrane protein found in Gram-negative bacteria, and is comprised of a large C-
467 terminal globular cytoplasmic domain linked to a single N-terminal transmembrane domain via an
468 extended linker[29,30]. FtsA and ZipA have overlapping functions but likely serve differing roles in
469 modulating division ring assembly[31,32]. Both FtsA and ZipA interact directly with FtsZ through an
470 interaction hub located at its C-terminal tail[33]. SepF is conserved in Gram-positive bacteria and
471 contains an N-terminal MTS and forms functional dimers, which interact with the C-terminal domain
472 of FtsZ[34,35]. In the Crenarchaeota, *Sulfolobus* CdvA links ESCRT-III (CdvB) proteins to the cell membrane
473 via direct interactions and is thought to assemble on the membrane surface[36].

474 Compared to these proteins, CdpA exhibits highest topological similarity to ZipA, suggesting an
475 analogous midcell anchor role. However, ZipA-GFP in *E. coli* showed clear movement around the
476 division ring[37], yet we found that CdpA-GFP remains relatively stable at mid-cell in *H. volcanii*,
477 suggesting they may operate via different mechanisms within the ring. SepF homologues from
478 different bacterial species can polymerize into large protein rings associated with cell wall
479 remodelling[38], whereas there is no evidence to show that archaeal SepF is capable of
480 polymerization[14,15]. Our discovery of CdpA as an archaeal division ring organisation and midcell
481 anchoring protein indicates that FtsZ assembly and its attachment to the membrane via a
482 transmembrane anchor are common and significant features shared by both the archaeal and
483 bacterial domains of life.

484 **Methods**

485 **Identification, phylogeny, and structural analysis of CdpA and CdpA-like sequences**

486 The reference amino acid sequence of HVO_0739 (CdpA) was first input into JackHMMER[39] to search
487 against UniProtKB database[40] with three iterations restricted by taxonomy in Archaea (taxid:2157).
488 The output HMM profile was used to scan the amino-acid sequences of all proteins in 1,587 high
489 quality diverse archaeal genomes from NCBI RefSeq database[41] with a significance threshold of an E-
490 value of 10^{-5}. The identified sequences were then confirmed using a BLASTP v2.13.0[42] search against
491 the reference CdpA sequence with an E-value cut-off of 10^{-5}; sequences giving no hit in the BLASTP
492 search result were removed. The remaining 1,336 sequences were taken as CdpA candidates. Of these,
493 proteins with a length between 80% to 120% of HVO_0739 (i.e., 260-400 residues) and with four
494 transmembrane segments (predicted using TMHMM v2.0)[43] within the N-terminal 75% of the
495 sequences were taken as CdpA family proteins (470 sequences), and the remaining 866 were
496 designated CdpA-like proteins.

497 Multiple alignment of the 470 CdpA sequences was then performed using MUSCLE v3.8.31[44]. A
498 neighbour-joining tree based on the amino-acid alignment was constructed using PHYLIP v3.698[45] with
499 the default model and 1,000 bootstrap replicates. HVO_2016 (*H. volcanii* CdpA-like protein) was
500 included as the outgroup to root the tree. The alignment was then reordered by tree structure. A
501 reduced version of the alignment was generated by removing columns that had a gap in the *H. volcanii*
502 CdpA reference sequence. This alignment was displayed using UGENE v46.0[46]. Taxonomy annotation
503 was based on the NCBI Taxonomy database. PsiPred v4.02[47] was used to estimate the secondary
504 structure of CdpA along the alignment.

505 Protein 3D structure predictions were downloaded in monomer form from the Alphafold structure
506 database (https://www.alphafold.ebi.ac.uk/entry/D4GTB2, accessed December 2023) or generated as
507 complexes using Alphafold v2.3.1 (Multimer)[48] using default settings with the full BFD reference
508 database. Structures were visualised and rendered with PyMOL[49] v2.5.1. Transmembrane topology
509 was predicted with Phobius[50].

510 **Growth of *H. volcanii* strains**

511 The *H. volcanii* cultures were grown in Hv-Cab medium[12,51]. Where necessary as auxotrophic
512 requirements, media were supplemented with uracil (50 µg/mL) for Δ*pyrE2* strains. To control gene
513 expression via the *p.tnaA* promoter, 0.2 mM or otherwise indicated concentration of L-tryptophan
514 (Sigma–Aldrich) was supplemented in these cultures. For microscopic imaging, the cultures were
515 incubated at 42°C with rotary shaking (200 rpm) and were maintained in log growth ($OD_{600} < 0.8$) for
516 at least 2 days before sampling for analysis of mid-log cultures. Representative data displayed in this
517 paper are representative of at least two independent biological replicate experiments.

518 **Construction of plasmids for gene deletion and genomic modification in *H. volcanii***

519 The plasmids, oligonucleotide sequences, and strains are given in the Supplementary Tables 1 and 2.
520 The plasmid pTA131 was used as the basis to construct the plasmids for gene deletion[52]. To make the
521 plasmid for *cdpA* deletion, the upstream and downstream flanks for homologous recombination on
522 either side of *cdpA* were PCR amplified from *H. volcanii* H26 genomic DNA, using the primers given in
523 Supplementary Table 1. The upstream flank fragment and downstream fragments were digested with
524 HindIII and BamHI, respectively, and cloned into pTA131 (at HindIII-BamHI) using Gibson assembly
525 reagents (NEB), resulting in pTA131_up_down_0739. The plasmids pTA131_CdpA_delNTD for N-
526 terminal domain (17-149 aa) deletion and pTA131_CdpA_delLinker for linker region deletion (150-284
527 aa) were obtained synthesised and cloned (Genscript). To make the plasmid pTA131_CdpA_delCTD
528 for C-terminal domain (285-328 aa) deletion, the upstream flank and downstream flanking fragments
529 of the CdpA C-terminal domain were amplified by using the primers in Supplementary Table 1 and
530 cloned into pTA131 (at HindIII-BamHI) using Gibson assembly (NEB) as described above.

531 Demethylated plasmids pTA131_up_down_0739, pTA131_CdpA_delNTD, pTA131_CdpA_delLinker,
532 and pTA131_CdpA_delCTD were used to transform *H. volcanni* H26 separately by using the pop-in-
533 pop-out method as described previously to delete the corresponding gene fragments[52]. Allele-
534 specific PCR was used to verify the expected deletion chromosomal structure, resulting in H26-base
535 strains carrying the *cdpA* mutations: Δ*cdpA*, $cdpA_{\Delta NTD}$, $cdpA_{\Delta Linker}$, and $cdpA_{\Delta CTD}$ (Supplementary Table
536 2).

537 **Construction of plasmids for gene expression in *H. volcanii***

538 The plasmids pTA962[53] or pIDJL40[12] (containing GFP) were used as the basis to construct plasmids for
539 controlled expression of the *cdpA* genes or modified versions. To construct pTA962-*cdpA*, the *cdpA*
540 ORF (HVO_0739) was amplified from *H. volcanii* H26 genomic DNA using primers HVO_0739_r and
541 HVO_0739_r, then the product was cloned between the NdeI and BamHI sites of pTA962. The *cdpA*
542 ORF was also amplified without its stop codon, then cloned between the NdeI and BamHI sites of
543 pIDJL40, to create the *cdpA*-gfp fusion. For dual expression of *cdpA*-gfp and *ftsZ1/2*-mCherry, PvuII
544 fragment of pTA962-*FtsZ1-mCherry* or *ftsZ2*-mCherry[13] (containing a *p.tnaA-ftsZ*-mCherry gene fusion)
545 were ligated into HindIII-cut (Klenow blunt-ended) pIDJL40_HVO_0739 containing (*cdpA*-GFP),
546 creating plasmid with two independent copies of the CdpA-GFP and FtsZ1/2-mCherry.

547 For expression of *cdpA*-GFP under its native promoter, the *cdpA* ORF, along with the intergenic region
548 of HVO_0739 and HVO_0738 (including native promotor of *cdpA*), was amplified using primers
549 CdpA_nativeP_F and HVO_0739 (NS)_r, then the product was cloned between ApaI and BamHI of
550 pIDJL40 (remove p.tnaA promoter).

551 To construct the $CdpA_{NTD}$-GFP fusion, the N-terminal domain of CdpA (1-149 aa) was amplified from
552 *H. volcanii* H26 genomic DNA using primers HVO_0739_f and CdpA_NTD_R, then the product was
553 cloned between NdeI and BamHI sites of pIDJL40. The mutant CdpA without the C-terminal domain
554 and without the N-terminal sequences were amplified from *H. volcanii* H26 and mutant $cdpA_{\Delta NTD}$
555 genomic DNA, respectively, by using the primers in Supplementary Table 1, and then cloned between
556 NdeI and BamHI sites of pIDJL40, to create $CdpA_{\Delta CTD}$-GFP and $CdpA_{\Delta NTD}$-GFP fusions. To construct
557 pHVID1-HA, synthetic DNA fragments encoding the HA tag with EcoRI and NotI overhangs were
558 obtained from Integrated DNA Technologies (IDT). These fragments were subsequently cloned into
559 the pHVID1 vector. To generate CdpA and FtsZ2 HA tagged plasmids, the respective genes amplified
560 from pIDJL40_*cdpA* and pIDJL40- *ftsZ2* were cloned between NdeI and BamHI sites of pHVID1-HA
561 plasmid, respectively. All plasmids were demethylated by passage through *E. coli* C2925 and re-
562 purified before transfer to *H. volcanii* H26 by polyethylene glycol-mediated spheroplast
563 transformation[52].

564 **Phase-contrast and epifluorescence microscopy**

565 A 2 µl sample of mid-log culture was loaded on a 1% agarose pad containing 18% buffered saltwater
566 (BSW) on a glass slide at room temperature, and a #1.5 glass coverslip was placed on top[13]. The images
567 were acquired on a GE DeltaVision Elite microscope with a pco.edge 5.5 sCMOS camara and an
568 Olympus 100X Plan Apo 1.4 NA objective using a FITC filter set (ex. 464-492 nm, em. 500-549 nm) or
569 an mCherry filter set (ex. 557-590, em. 598-617 nm).

570 The analysis of cell shape (area vs circularity), FtsZ1-mCherry intensity ratio (localized/diffuse
571 fluorescence), and FtsZ1-mCherry localization thickness measurements were performed as
572 described[13]. For counting the number of FtsZ2-GFP rings per cell, the number of correctly positioned
573 rings were manually counted to exclude the abnormal localizations, and cell length was determined
574 by a custom script in FIJI[13].

575 The measurement of localized and diffuse FtsZ1- and FtsZ2-FP fluorescence areas were analyzed in
576 MATLAB 2019b (MathWorks). The phase-contrast images were first pre-processed using a bottom-hat
577 transform (*imbothat* function) with a disk-shaped structuring element of a radius of 30 pixels for the

578 kernel. These were binarized and individual cells were segmented (*bwconncomp* function). Cell debris
579 were excluded by removing objects with area less than 1 μm^2 (~237 pixels). The filtered cell outline
580 was parametrically smoothed by fitting each component of cell outline (i.e., x- and y-components in
581 the Cartesian coordinate system) with two Fourier expansions up to the 8th order mode. The
582 corresponding fluorescence images were pre-treated by subtracting the average intensity of the
583 background (i.e., excluding regions of the detected cells). Additionally, a top-hat transform (*imtophat*
584 function) was applied with a disk-shaped structuring element of a radius of 10 pixels. FtsZ1 and FtsZ2
585 clusters within each cell were identified and segmented by converting the processed fluorescence
586 images to 8-bit and applying the extended-maxima transform (*imextendedmax* function) with a
587 threshold value of 1. Small fluctuations in FtsZ1-FP and FtsZ2-FP fluorescence signals were neglected
588 by removing clusters less than 4 pixels. The localization area of FtsZ1 and FtsZ2 in each cell was then
589 defined as the total area of all FtsZ1 or FtsZ2 clusters found within the cell outline. The ratio of FtsZ2
590 localization area to FtsZ1 localization area was then determined for each cell. Cells were excluded
591 from the analysis if either FtsZ1 or FtsZ2 clusters were undetectable within the cell or if the cell
592 exhibited a signal-to-noise ratio of less than 2.

593 CdpA-GFP localization along the medial axis in filamentous SepF depleted cells was analysed using the
594 same segmentation approach described above with MATLAB. After rolling ball background subtraction
595 (radius: 20 pixels, ~1.4 µm), CdpA-GFP intensities were mapped along the medial axis by averaging
596 pixel intensity along the transverse direction and smoothed using a moving average filter (window
597 size: 10 pixels, ~0.7 µm). Peak localizations of CdpA were identified using the *findpeaks* function and
598 manually corrected to avoid foci or other aberrant structures.

599 **Time-lapse Microscopy**

600 The sample was prepared by using submerged sandwich technique as previously described[13]. A 2 µl
601 sample of mid-log culture was placed on a 0.3% w/v agarose pad (containing the medium for the
602 growth) prepared on an 8-mm glass-based (#1.5) FluoroDish (WPI). A 4 mL volume of medium was
603 added to the FluoroDish to cover the agarose pad assembly, and the lid was placed on the FluoroDish
604 to minimize evaporation. The images were captured at 42°C every 10 min for 24 h on a Nikon TiE2
605 inverted fluorescence microscope with a 100 X oil-immersion phase-contrast NA 1.45 objective.

606 **2D- and 3D-Structured Illumination Microscopy (SIM)**

607 Samples were prepared on agarose pads as described above for phase-contrast and epifluorescence
608 microscopy. Images were captured on a Delta Vision OMX SR 3D Structured Illumination Microscope
609 with a 60 X Plan 1.42 NA Oil Immersion Objective at room temperature for visualizing fluorescent
610 fusion proteins, or at 42°C for 3D-SIM time-lapse imaging. GFP and mCherry signals were collected
611 through a FITC and a TRITC filter, respectively. 3D-SIM images were sectioned using a 125 nm z-step.
612 The reconstructed images-stacks were 3D rendered and visualized by using IMARIS x64 9.6.0 (Bitplane
613 Scientific). The maximum diameters of FtsZ2-GFP nano-rings were manually measured using the
614 "Measurement Points" function in IMARIS. 3D-SIM time series (acquired every 30 s – 2 min as required)
615 were compiled from single time points using IMARIS to create a time-lapse series, followed by bleach
616 correction (Histogram Match) and registration (using 'translation' in TurboReg) in Image J 1.53v. The
617 3D intensity plots were generated by using '3D surface plot" in ImageJ 1.53v. Two regions of interest
618 were monitored overtime show how FtsZ-GFP or CdpA-GFP fluorescence fluctuates in the Z ring.

619 **Total Internal Reflection fluorescence (TIRF) microscopy**

620 Samples were prepared as described for time-lapse microscopy. The TIRF imaging was performed
621 using a Nikon TiE-2 N-STORM microscope operated in TIRF mode on a stage top incubator (OKO-lab)
622 set to 42°C, equipped with a 100 X 1.49 NA TIRF objective. The TIRF angle was set to optimize the
623 signal to noise ratio at a fixed angle of 100°. The imaging settings were chosen to minimize

624 photobleaching with the power intensity set at 5% and the exposure time was 150 – 200 ms. FtsZ1-
625 GFP was imaged at 4 s intervals for 15 min, and FtsZ2-GFP were imaged at 10 s intervals for 40 min.
626 CdpA-GFP was imaged either at 4 second intervals for 15 min or 10 second intervals for 40 min.

627 For the analysis of TIRF data[5], fluorescence images were stabilized, and registered (StackReg,
628 Translation), and corrected for photobleaching (simple ratio), interpolated to 20 nm/pixel via the
629 bicubic method in Image J, and moving averaged over a 12-frame window of time. The fluorescence
630 intensity of an FtsZ polymer along the direction of its movement in each frame was determined from
631 the intensity along a line with a width of 25 interpolated pixels (~ 500 nm) manually drawn across the
632 full length of the path of the FtsZ polymer. This line was then used to plot the kymograph (line width
633 = 25) then background subtraction rolling ball =25, and smooth (for display purpose). The speeds of
634 clusters were calculated by manually measuring the slopes of leading and trailing edges of clear
635 fluorescence zigzags in the kymograph. The distributions of speed of FtsZ-FP clusters were plotted in
636 OrginPro (2021). For analysis of Z-ring intensity fluctuations during TIRF time-lapse imaging, briefly, a
637 cell of interest was cropped out from both fluorescence and bright-field images. Second, the cell was
638 rotated to align the Z-ring horizontally. Fluorescence background within the cell was calculated by
639 averaging the total integrated intensity over the area defined by the cell contour. A square region of
640 interest (ROI) with 3×3 pixels in the centre of the ring was then chosen manually. The corrected
641 intensity was calculated as the integrated intensity within the ROI after background subtraction and
642 smoothed by a moving-average filter with a window size of 5 time points in OriginPro (2021).
643
644 The Power Spectral Density (PSD) analysis was conducted using custom MATLAB scripts. Firstly, a cell
645 of interest was cropped out from both fluorescence and bright-field images. The fluorescence images
646 were then registered to the bright-field image and corrected for sample/stage drift and
647 photobleaching. Following this, the cell was rotated manually to align the Z-ring horizontally. To
648 determine fluorescence background within the cell, the total integrated intensity over the area
649 defined by the cell outline was averaged. A square region of interest (ROI) with 3×3 pixels at the center
650 of the ring was then chosen manually. The local FtsZ-GFP (I) was computed as the integrated intensity
651 within the ROI after background subtraction.

652 Using fluorescence intensity time trace, $I(t)$, from the center of the division ring, the PSD curves were
653 calculated. This involved subtracting the mean value $\langle I(t)\rangle$ from $I(t)$ and subsequently applying the
654 Fast-Fourier Transform (FFT) to the shifted time trace (fft function in MATLAB). For each cell, the PSD
655 curve across different frequencies f was then calculated as follows:

656 $$PSD(f) = \frac{|FFT(I(t) - \langle I(t)\rangle)|}{n\Delta f \cdot Var(I(t))},$$

657 where n is the total number of frames of the trace and Δf is the frame rate ($1/4\ s^{-1}$). Note that the
658 PSD was normalized by the squared magnitude of the intensity trace (variance of $I(t)$). The mean PSD
659 curves were generated by averaging the PSD curves of individual cells in each strain.

660 **Immunoprecipitation of HA-tagged CdpA**

661 The method was based on that described[14] but with modifications. H26-HA and CdpA-HA strains were
662 grown in 300 mL of Hv-cab medium supplemented with 2 mM Trp until their OD_{600} reached 0.5. The
663 cells were harvested by centrifugation at 6,000 x g for 15 min. The pelleted cells were resuspended in
664 30 mL of 18% buffered salt water supplemented with 10 mM HEPES. For crosslinking 1.5% (w/v)
665 formaldehyde was added to the cell suspension, and the mixture was incubated at room temperature
666 for 10 min with constant shaking. The crosslinking reaction was stopped by adding 20 mL of 18%
667 buffered salt-water containing 1.25 M glycine. The cells were centrifuged again for 15 min at 6,000 x
668 g. The cell pellet was washed twice with 18% buffered salt water with 1.25 M glycine. After the final
669 wash, the cell pellet was resuspended in 3 mL of lysis buffer (1X PBS, 10 mM MgCl2, 10 µg/ml DNase

670 I and protease inhibitor cocktail). The cells where lysed by sonication for 5 min, with 5 sec on and 5
671 sec off cycle at 35% amplitude. To remove the cell debris, lysed cells were centrifuged at 6,000 g for
672 15 min at 4 °C in a microcentrifuge. The supernatant, expected to contain cytosolic and fragmented
673 membrane fractions, was used for immunoprecipitation with washed anti-HA magnetic beads
674 (Thermo Scientific) as described in the manufacturer's instructions. Briefly, the supernatant (1 mL)
675 was added to 0.5 mg of anti-HA beads and incubated at room temperature for 30 min with gentle
676 mixing. The beads were washed twice with buffer (Tris–buffered saline with 0.05% Tween-20) and
677 proteins were eluted with 0.1 M glycine pH 2.0, and then neutralized and denatured by boiling for 5
678 min with SDS sample buffer, which was also expected to disrupt crosslinking.

679 **Western blotting**

680 Proteins were separated by sodium dodecyl-sulphate polyacrylamide gel electrophoresis (SDS-PAGE)
681 and then electro-transferred to a nitrocellulose membrane using a Bio-Rad trans-blot turbo transfer
682 system. The membrane was blocked overnight in 5% (w/v) skim milk in Tris-buffered saline with 0.05%
683 Tween-20 (TBST). A primary antibody recognizing heamagglutanin (HA) (Thermo Fisher Scientific, Cat#
684 26183) (1:10,000), FtsZ1[13] (1:1,000) and FtsZ2[13] (1:2,000) were incubated with membrane for 2 h with
685 constant shaking at RT. Following that the membrane was washed three times, 5 min each with
686 constant shaking at RT, with TBST. The membrane was then incubated with the secondary antibody
687 against mouse (Goat anti-mouse IgG-HRP; AbCam 6789) for 1 h in a 1:5,000 dilution. The membrane
688 was washed five times (5 min each) with TBST before detection. Bands were detected with enhanced
689 chemiluminescence reagents (Thermo-Fisher) using an Amersham Imager 600 system.

690 **Mass spectrometry (MS)**

691 Fifty micrograms of eluted proteins from the pull-down assay were subjected to trypsin digestion using
692 Promega Trypsin Gold, mass spectrometer grade (1 µg/µL) in 50 mM acetic acid. The digested samples
693 were processed for clean-up using solid-phase extraction (SPE). An equivalent amount of protein (15
694 µg) for each sample was loaded onto the SPE columns, which were then washed, and peptides eluted.
695 Columns were manually prepared using Empore SDS-RPS (Styrenedivinylbenzene reverse phase
696 sulfonate) with a pipette tip. The SDB-RPS based tips were used for peptide clean up.

697 Eluted samples were dried in a vacuum centrifuge, and peptides were reconstituted in the injection
698 solvent suitable for the LC/MS system. Analysis was performed on a Q Exactive Plus mass
699 spectrometer (Thermo Fisher Scientific), and the MS/MS data files were analyzed using PEAKS Studio
700 against *Haloferax volcanii* predicted proteome database using Uniprot. The MS peak areas obtained
701 for the peptides were then used for statistical analyses.

702 **Data availability**

703 The data generated in this study, including microscopy image analyses and western blots are provided
704 in the Supplementary Information and Source data files with this paper. The mass spectrometry
705 proteomics data have been deposited to the ProteomeXchange Consortium via the PRIDE[54] partner
706 repository with the dataset identifier PXD062651. Other data and biological materials are available
707 from the corresponding author upon reasonable request.

708 **References**

709 1 Adams, D. W. & Errington, J. Bacterial cell division: assembly, maintenance and disassembly
710 of the Z ring. *Nature Reviews Microbiology* **7**, 642-653 (2009).
711 2 Osawa, M. & Erickson, H. P. Liposome division by a simple bacterial division machinery.
712 *Proceedings of the National Academy of Sciences* **110**, 11000-11004 (2013).
713 3 Szwedziak, P., Wang, Q., Bharat, T. A., Tsim, M. & Löwe, J. Architecture of the ring formed by
714 the tubulin homologue FtsZ in bacterial cell division. *Elife* **3**, e04601 (2014).
715 4 Bisson-Filho, A. W. *et al.* Treadmilling by FtsZ filaments drives peptidoglycan synthesis and
716 bacterial cell division. *Science* **355**, 739-743 (2017).
717 5 Yang, X. *et al.* GTPase activity–coupled treadmilling of the bacterial tubulin FtsZ organizes
718 septal cell wall synthesis. *Science* **355**, 744-747 (2017).
719 6 Nogales, E. Structural insights into microtubule function. *Annual review of biophysics and*
720 *biomolecular structure* **30**, 397-420 (2001).
721 7 Wade, R. H. On and around microtubules: an overview. *Molecular biotechnology* **43**, 177-191
722 (2009).
723 8 Roll-Mecak, A. The tubulin code in microtubule dynamics and information encoding.
724 *Developmental cell* **54**, 7-20 (2020).
725 9 Aylett, C. H. & Duggin, I. G. The tubulin superfamily in archaea. *Prokaryotic Cytoskeletons:*
726 *Filamentous Protein Polymers Active in the Cytoplasm of Bacterial and Archaeal Cells*, 393-417
727 (2017).
728 10 Liao, Y., Ithurbide, S., de Silva, R. T., Erdmann, S. & Duggin, I. G. Archaeal cell biology: diverse
729 functions of tubulin-like cytoskeletal proteins at the cell envelope. *Emerging Topics in Life*
730 *Sciences* **2**, 547-559 (2018).
731 11 Vaughan, S., Wickstead, B., Gull, K. & Addinall, S. G. Molecular evolution of FtsZ protein
732 sequences encoded within the genomes of archaea, bacteria, and eukaryota. *Journal of*
733 *molecular evolution* **58**, 19-29 (2004).
734 12 Duggin, I. G. *et al.* CetZ tubulin-like proteins control archaeal cell shape. *Nature* **519**, 362-365
735 (2015).
736 13 Liao, Y., Ithurbide, S., Evenhuis, C., Löwe, J. & Duggin, I. G. Cell division in the archaeon
737 Haloferax volcanii relies on two FtsZ proteins with distinct functions in division ring assembly
738 and constriction. *Nature microbiology* **6**, 594-605 (2021).
739 14 Nussbaum, P., Gerstner, M., Dingethal, M., Erb, C. & Albers, S. V. The archaeal protein SepF is
740 essential for cell division in Haloferax volcanii. *Nat Commun* **12**, 3469 (2021).
741 https://doi.org:10.1038/s41467-021-23686-9
742 15 Pende, N. *et al.* SepF is the FtsZ anchor in archaea, with features of an ancestral cell division
743 system. *Nature Communications* **12**, 3214 (2021).
744 16 Nussbaum, P. *et al.* Proteins containing photosynthetic reaction centre domains modulate
745 FtsZ-based archaeal cell division. *Nat Microbiol* **9**, 698-711 (2024).
746 https://doi.org:10.1038/s41564-024-01600-5
747 17 Zhao, S. *et al.* Widespread photosynthesis reaction centre barrel proteins are necessary for
748 haloarchaeal cell division. *Nat Microbiol* **9**, 712-726 (2024). https://doi.org:10.1038/s41564-
749 024-01615-y
750 18 Darnell, C. L. *et al.* The ribbon-helix-helix domain protein CdrS regulates the tubulin homolog
751 ftsZ2 to control cell division in archaea. *MBio* **11**, 10.1128/mbio. 01007-01020 (2020).
752 19 Liao, Y. *et al.* CdrS is a global transcriptional regulator influencing cell division in Haloferax
753 volcanii. *Mbio* **12**, 10.1128/mbio. 01416-01421 (2021).
754 20 Braun, F. *et al.* Cyclic nucleotides in archaea: Cyclic di-AMP in the archaeon Haloferax volcanii
755 and its putative role. *Microbiologyopen* **8**, e00829 (2019). https://doi.org:10.1002/mbo3.829
756 21 Schiller, H. *et al.* Identification of structural and regulatory cell-shape determinants in
757 Haloferax volcanii. *Nat Commun* **15**, 1414 (2024). https://doi.org:10.1038/s41467-024-45196-
758 0

22 Ithurbide, S., de Silva, R. T., Brown, H. J., Shinde, V. & Duggin, I. G. A vector system for single and tandem expression of cloned genes and multi-colour fluorescent tagging in Haloferax volcanii. *Microbiology (Reading)* **170** (2024). https://doi.org:10.1099/mic.0.001461

23 Mills, J. *et al.* Extracellular vesicle formation in Euryarchaeota is driven by a small GTPase. *Proc Natl Acad Sci U S A* **121**, e2311321121 (2024). https://doi.org:10.1073/pnas.2311321121

24 Addinall, S. G. & Lutkenhaus, J. FtsA is localized to the septum in an FtsZ-dependent manner. *Journal of bacteriology* **178**, 7167-7172 (1996).

25 Beall, B. & Lutkenhaus, J. Impaired cell division and sporulation of a Bacillus subtilis strain with the ftsA gene deleted. *Journal of bacteriology* **174**, 2398-2403 (1992).

26 Nußbaum, P., Gerstner, M., Dingethal, M., Erb, C. & Albers, S.-V. The archaeal protein SepF is essential for cell division in Haloferax volcanii. *Nature communications* **12**, 3469 (2021).

27 Pichoff, S. & Lutkenhaus, J. Tethering the Z ring to the membrane through a conserved membrane targeting sequence in FtsA. *Molecular microbiology* **55**, 1722-1734 (2005).

28 Pichoff, S. & Lutkenhaus, J. Identification of a region of FtsA required for interaction with FtsZ. *Molecular microbiology* **64**, 1129-1138 (2007).

29 Mosyak, L. *et al.* The bacterial cell-division protein ZipA and its interaction with an FtsZ fragment revealed by X-ray crystallography. *The EMBO journal* **19**, 3179-3191 (2000).

30 Moy, F. J., Glasfeld, E., Mosyak, L. & Powers, R. Solution structure of ZipA, a crucial component of Escherichia coli cell division. *Biochemistry* **39**, 9146-9156 (2000).

31 Cameron, T. A., Vega, D. E., Yu, C., Xiao, H. & Margolin, W. ZipA uses a two-pronged FtsZ-binding mechanism necessary for cell division. *Mbio* **12**, e02529-02521 (2021).

32 Pichoff, S. & Lutkenhaus, J. Unique and overlapping roles for ZipA and FtsA in septal ring assembly in Escherichia coli. *The EMBO journal* (2002).

33 Ortiz, C., Natale, P., Cueto, L. & Vicente, M. The keepers of the ring: regulators of FtsZ assembly. *FEMS microbiology reviews* **40**, 57-67 (2016).

34 Hamoen, L. W., Meile, J. C., De Jong, W., Noirot, P. & Errington, J. SepF, a novel FtsZ-interacting protein required for a late step in cell division. *Molecular microbiology* **59**, 989-999 (2006).

35 Sogues, A. *et al.* Essential dynamic interdependence of FtsZ and SepF for Z-ring and septum formation in Corynebacterium glutamicum. *Nature communications* **11**, 1641 (2020).

36 Samson, R. Y. *et al.* Molecular and structural basis of ESCRT-III recruitment to membranes during archaeal cell division. *Mol Cell* **41**, 186-196 (2011). https://doi.org:10.1016/j.molcel.2010.12.018

37 Söderström, B., Chan, H., Shilling, P. J., Skoglund, U. & Daley, D. O. Spatial separation of FtsZ and FtsN during cell division. *Molecular microbiology* **107**, 387-401 (2018).

38 Wenzel, M. *et al.* Control of septum thickness by the curvature of SepF polymers. *Proceedings of the National Academy of Sciences* **118**, e2002635118 (2021).

39 Johnson, L. S., Eddy, S. R. & Portugaly, E. Hidden Markov model speed heuristic and iterative HMM search procedure. *BMC bioinformatics* **11**, 1-8 (2010).

40 Coudert, E. *et al.* Annotation of biologically relevant ligands in UniProtKB using ChEBI. *Bioinformatics* **39**, btac793 (2023).

41 O'Leary, N. A. *et al.* Reference sequence (RefSeq) database at NCBI: current status, taxonomic expansion, and functional annotation. *Nucleic acids research* **44**, D733-D745 (2016).

42 Camacho, C. *et al.* BLAST+: architecture and applications. *BMC bioinformatics* **10**, 1-9 (2009).

43 Krogh, A., Larsson, B., Von Heijne, G. & Sonnhammer, E. L. Predicting transmembrane protein topology with a hidden Markov model: application to complete genomes. *Journal of molecular biology* **305**, 567-580 (2001).

44 Edgar, R. C. MUSCLE: multiple sequence alignment with high accuracy and high throughput. *Nucleic acids research* **32**, 1792-1797 (2004).

45 Felsenstein, J. *PHYLIP (phylogeny inference package), version 3.5 c*. (Joseph Felsenstein., 1993).

46 Okonechnikov, K., Golosova, O., Fursov, M. & Team, U. Unipro UGENE: a unified bioinformatics toolkit. *Bioinformatics* **28**, 1166-1167 (2012).
47 Buchan, D. W. & Jones, D. T. The PSIPRED protein analysis workbench: 20 years on. *Nucleic acids research* **47**, W402-W407 (2019).
48 Jumper, J. *et al.* Highly accurate protein structure prediction with AlphaFold. *nature* **596**, 583-589 (2021).
49 Schrodinger, L. The PyMOL molecular graphics system. *Version* **1**, 8 (2015).
50 Kall, L., Krogh, A. & Sonnhammer, E. L. Advantages of combined transmembrane topology and signal peptide prediction--the Phobius web server. *Nucleic Acids Res* **35**, W429-432 (2007). https://doi.org:10.1093/nar/gkm256
51 de Silva, R. T. *et al.* Improved growth and morphological plasticity of Haloferax volcanii. *Microbiology (Reading)* **167** (2021). https://doi.org:10.1099/mic.0.001012
52 Allers, T., Ngo, H.-P., Mevarech, M. & Lloyd, R. G. Development of additional selectable markers for the halophilic archaeon Haloferax volcanii based on the leuB and trpA genes. *Applied and environmental microbiology* **70**, 943-953 (2004).
53 Allers, T., Barak, S., Liddell, S., Wardell, K. & Mevarech, M. Improved strains and plasmid vectors for conditional overexpression of His-tagged proteins in Haloferax volcanii. *Applied and environmental microbiology* **76**, 1759-1769 (2010).
54 Perez-Riverol, Y. *et al.* The PRIDE database at 20 years: 2025 update. *Nucleic Acids Research* **53**, D543-D553 (2025).

Acknowledgments

This study was supported by the University of Technology Sydney Chancellor's Research Fellowship (PR021-13161 to Y.L.) and by the Australian Research Council (FT160100010 to I.G.D, DP220101143 to B.S., and DP250100999 to I.G.D & Y.L.). For technical and facilities management support, we thank Matthew Padula from the Proteomics Core Facility, UTS, Pauline Coulon for assistance with proteomics data handling, Matthew Pittorino for discussion of TIRF image analysis, and Amy Bottomley, Christian Evenhuis, and Louise Cole from the Microbial Imaging Facility, UTS. We thank Sonja-Verena Albers at the University of Freiburg for providing the *sepF* depletion strain (HTQ239) and plasmid for expression of *sepF-GFP* (pSVA3942).

Author Contributions Statement

Y.L and I.G.D. designed the research. Y.L. constructed most of the plasmids, strains and conducted the primary microscopy imaging and analyses. V.D.S constructed plasmids and strains for pull-down experiments and performed immunoprecipitation, western blot and mass-spectrometry analyses. D.H performed phylogeny analysis of CdpA and CdpA-like sequences and contributed the production of some image analysis figures using R programming. Z.X. performed PSD analysis and quantified the localization area of FtsZ1/FtsZ2 and ring number of CdpA-GFP in HTQ239 strain in MATLAB. B.S. contributed to the TIRF imaging. K.A.M, and I.G.D. performed Alphafold2 Multimer prediction and analysis. Y.L. and I.G.D. interpreted results and wrote the original draft. All authors reviewed and gave scientific input to revise the manuscript. Y.L and I.G.D managed and supervised the project and acquired funding.

Competing Interests Statement

The authors declare no competing interests.

854 **Figures**

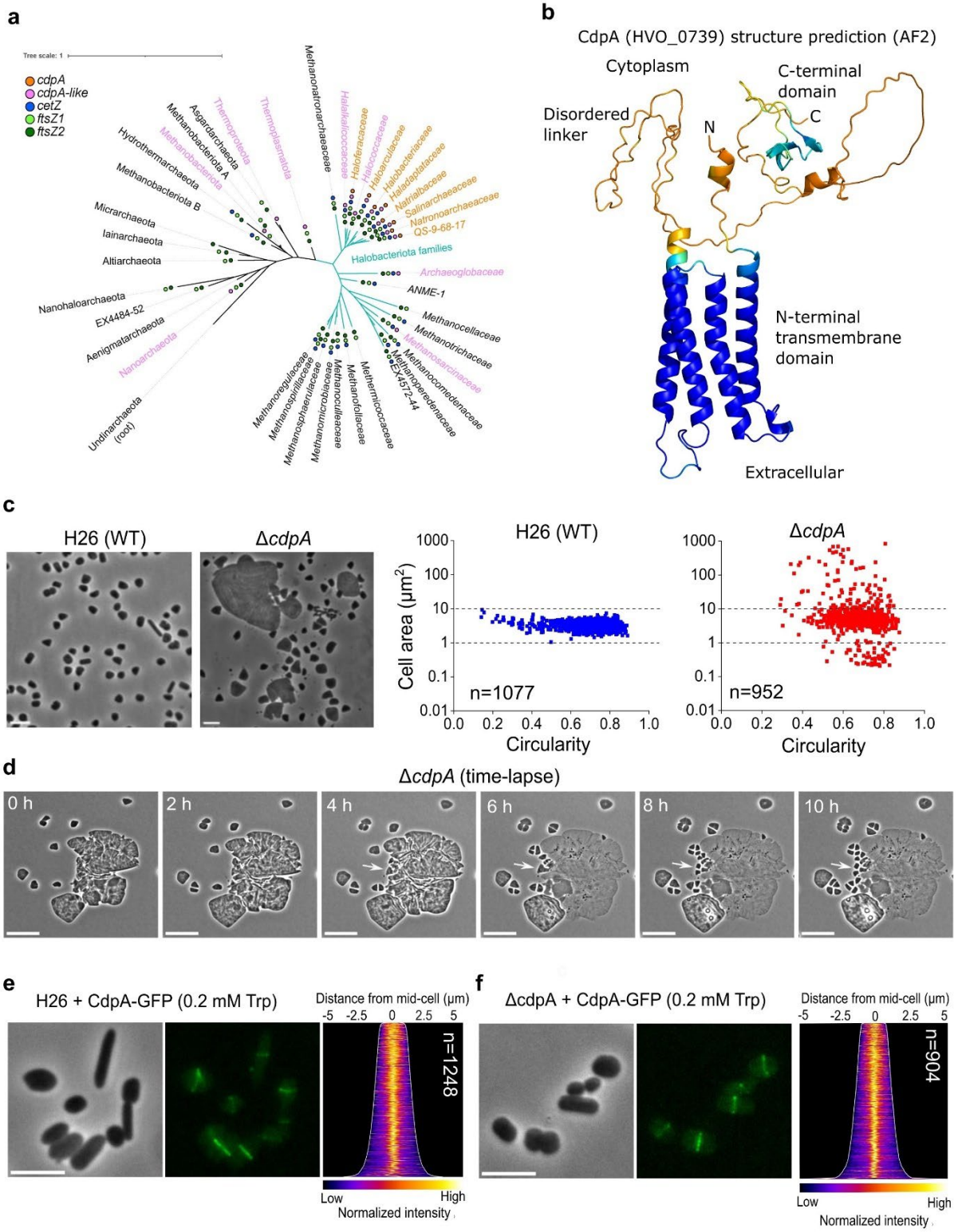

855

856 **Fig. 1. CdpA is cell division protein in haloarchaea. a,** Phylogenetic distribution of CdpA (orange
857 circles), CdpA-like (pink), CetZ (blue), FtsZ1 (light green), and FtsZ2 (dark green) on a schematic
858 reference phylogeny of the Archaea (Genome Taxonomy Database, release 207), expanding on
859 Halobacteriota families. The presence /absence is shown at the indicated taxonomic level and is
860 marked as present if identified in at least one genome within that taxon. **b,** Alphafold2 prediction of

861 CdpA monomer structure coloured by model confidence (blue - pLDDT > 90%, orange - pLDDT <
862 50%) and predicted overall membrane topology. **c**, Phase-contrast microscopy of wild-type (WT) and
863 Δ*cdpA* strains in steady mid-log cultures and the corresponding cell shape analysis. n= number of
864 cells examined over one biologically independent experiment. The data shown is representative of at
865 least two independent experiments. Source data are provided as a Source Data file. **d,** Live-cell time-
866 lapse images of Δ*cdpA* growing on an agarose media pad and showing cell lysis, fragmentation, and
867 division processes (arrows). **e**, **f,** Phase-contrast and fluorescence micrographs of wild-type cells
868 expressing CdpA-GFP (**e**) and Δ*cdpA* expressing CdpA-GFP (**f**) under control of the *p.tnaA* promoter
869 with 0.2 mM Trp induction. Demographic analysis (righthand panels) showing fluorescence intensity
870 along the long axis ordered by cell lengths, top to bottom. n= number of cells examined over one
871 biologically independent experiment. The data shown in panel d, e, f is representative of at least two
872 independent experiments. All scale bars, 5 µm.

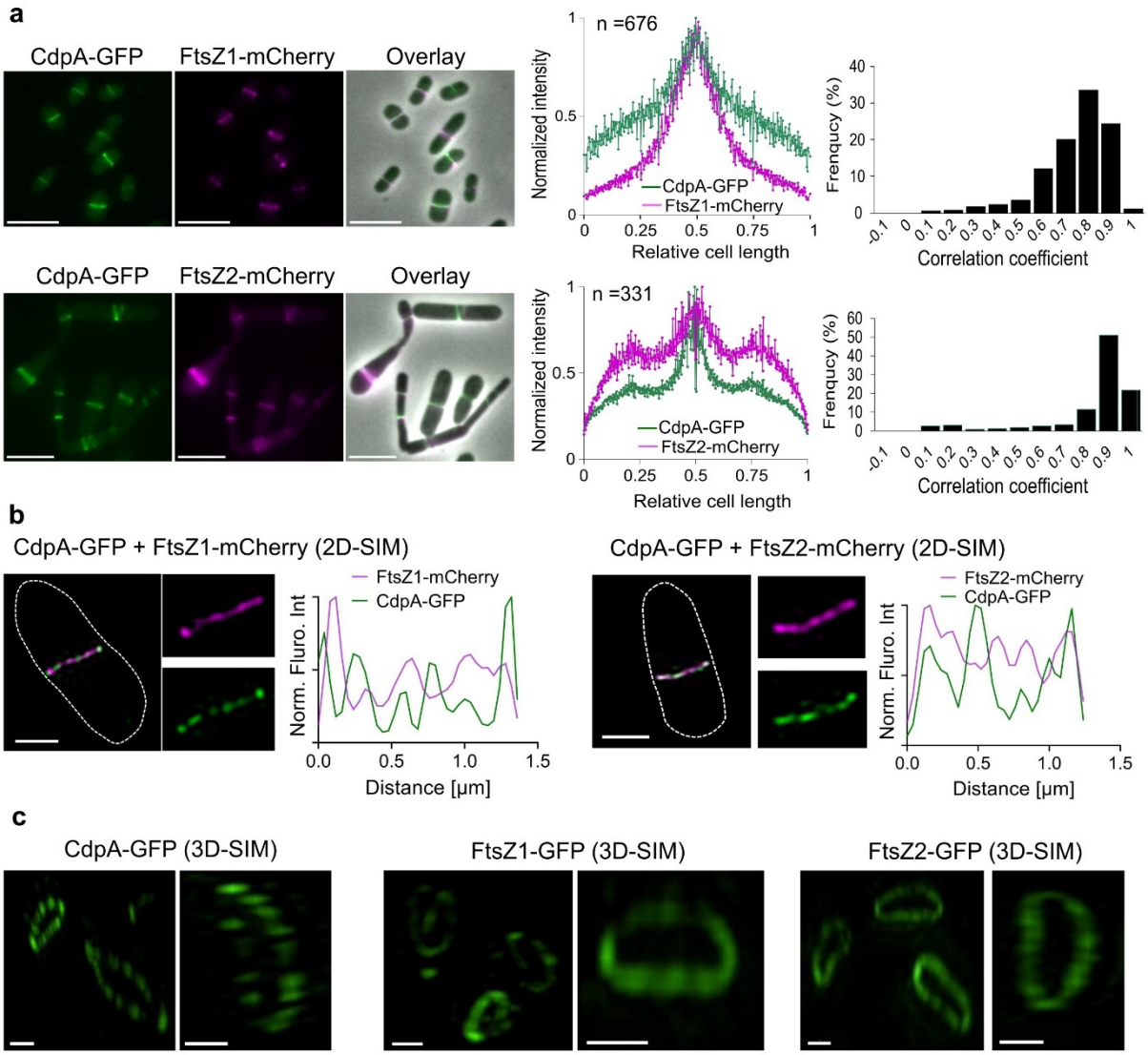

Fig. 2. Sub-cellular and sub-ring localization of CdpA with FtsZ1 or FtsZ2. a, Phase-contrast and fluorescence images of *H. volcanii* strains YL6 (H26 + CdpA-GFP + FtsZ1-mCherry dual expression) and YL7 (H26 + CdpA-GFP + FtsZ2-mCherry dual expression) cultured with 0.2 mM Trp during mid-log growth. The middle graphs show the intensity profile of the fluorescence signal (magenta for mCherry, and green for GFP) by plotting the normalized median intensity perpendicular to the long axis of cells. The right graphs show correlation coefficients plotted as a frequency distribution. n = number of cells examined over one independent experiment. The data shown are representative of at least two independent experiments. Scale bars, 5 µm. Source data are provided as a Source Data file. **b,** Dual-colour of 2D-SIM images of mid-log *H. volcanii* YL6 and YL7 grown with 0.2 mM Trp. mCherry (magenta) and GFP (green) fluorescence was quantified by plotting normalized intensity in the respective channel along the ring band. Scale bars, 1 µm. Source data are provided as a Source Data file. **c,** 3D-SIM images (xy-tilted) of mid-log *H. volcanii* YL29 (H26 + CdpA-GFP), YL24 (H26 + FtsZ1-GFP), and YL26 (H26 + FtsZ2-GFP) grown with 0.2 mM Trp. Scale bars, 0.5 µm. The data shown in panel b and c are representative of at least two independent experiments.

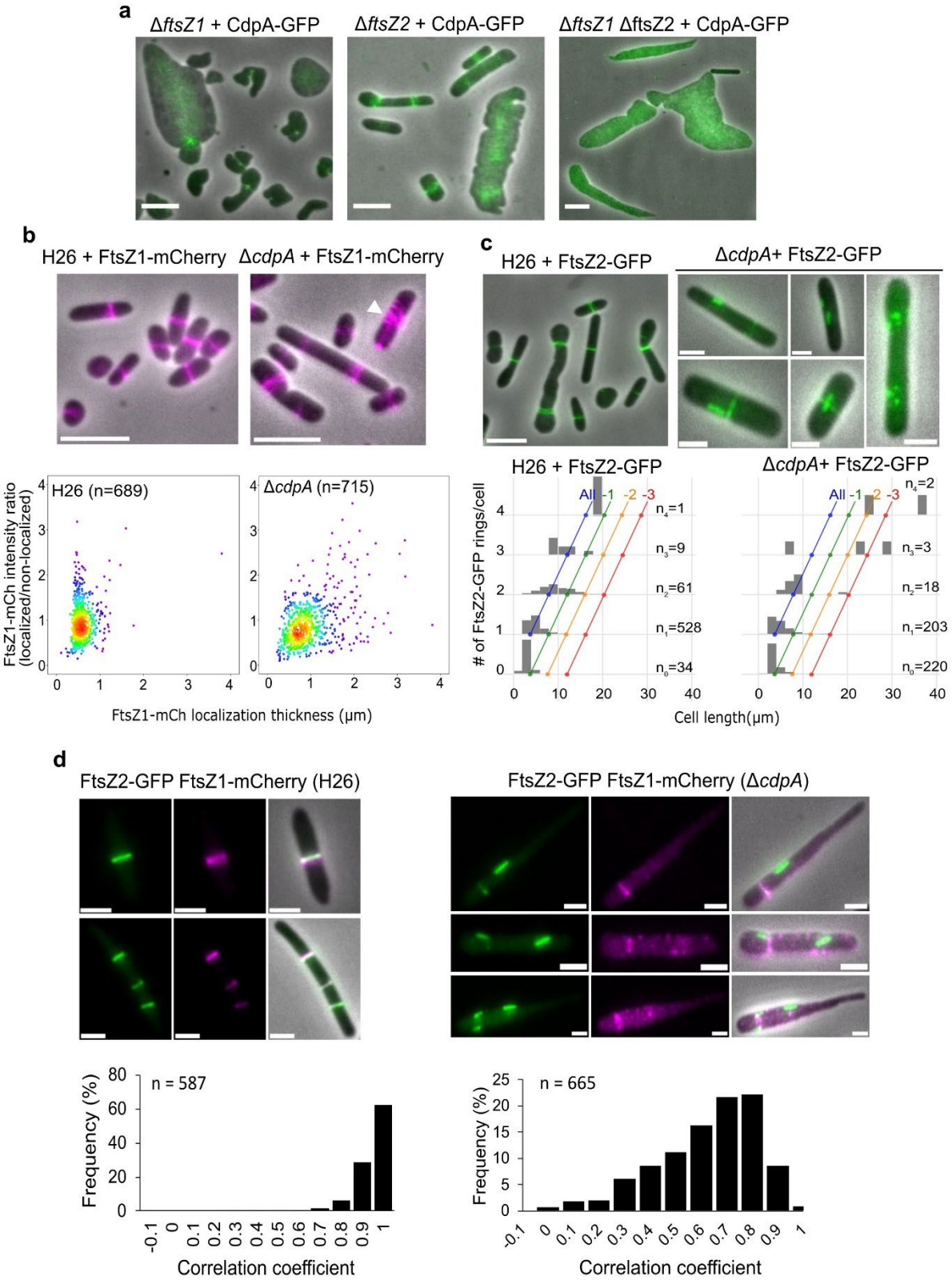

Fig. 3. CdpA, FtsZ1 and FtsZ2 show different localization interdependencies and strongly influence each other's midcell structures. All strains were grown in Hv-Cab medium with SepF, and mid-log cultures were sampled for microscopy. **a,** Phase-contrast and fluorescence composite images of CdpA-GFP in the absence of FtsZ1, FtsZ2, or both. Scale bars, 5 µm. The micrographs shown are representative of at least two independent experiments. **b,** Left: localization of FtsZ1-mCherry in wild-

type H26 and Δ*cdpA* backgrounds. The arrowhead indicates a poorly condensed FtsZ1-mCherry structure in Δ*cdpA*. Scale bars, 5 µm. The dot-plots show quantification of the degree of FtsZ1-mCherry localization versus individual localization thickness as a measurement of protein condensation along the long axis in the indicated backgrounds. The data points are coloured with a proximity heatmap. **c,** localization of FtsZ2-GFP in H26 (scale bar, 5 µm) and Δ*cdpA* backgrounds (scale bars, 2 µm). The histograms show the number of FtsZ2-GFP structures detected versus cell length in the indicated backgrounds. Blue diagonals ("All") represent 1 localization per 4 µm in length (i.e. approximately equivalent to all division sites detected at the normal frequency per cell length in wild-type cells), green ("-1") indicates one fewer rings/cell length, yellow is two fewer, and red is 3 fewer. n_x=number of cells for the indicated number(x) of localizations examined over one biologically independent experiment. **d,** Upper: localization of FtsZ1-mCherry and FtsZ2-GFP in H26 and Δ*cdpA* strains. Scale bars, 2 µm, Bottom: correlation coefficient between FtsZ1-mCherry and FtsZ2-GFP plotted as a frequency distribution. The majority (97%) of H26 cells had a correlation coefficient of ≥0.8, while only 32% of Δ*cdpA* cells had a correlation coefficient of ≥0.8. For panel b, c, and d, n= number of cells examined over one biologically independent experiment, and the data shown is representative of at least two independent experiments. Source data are provided as a Source Data file.

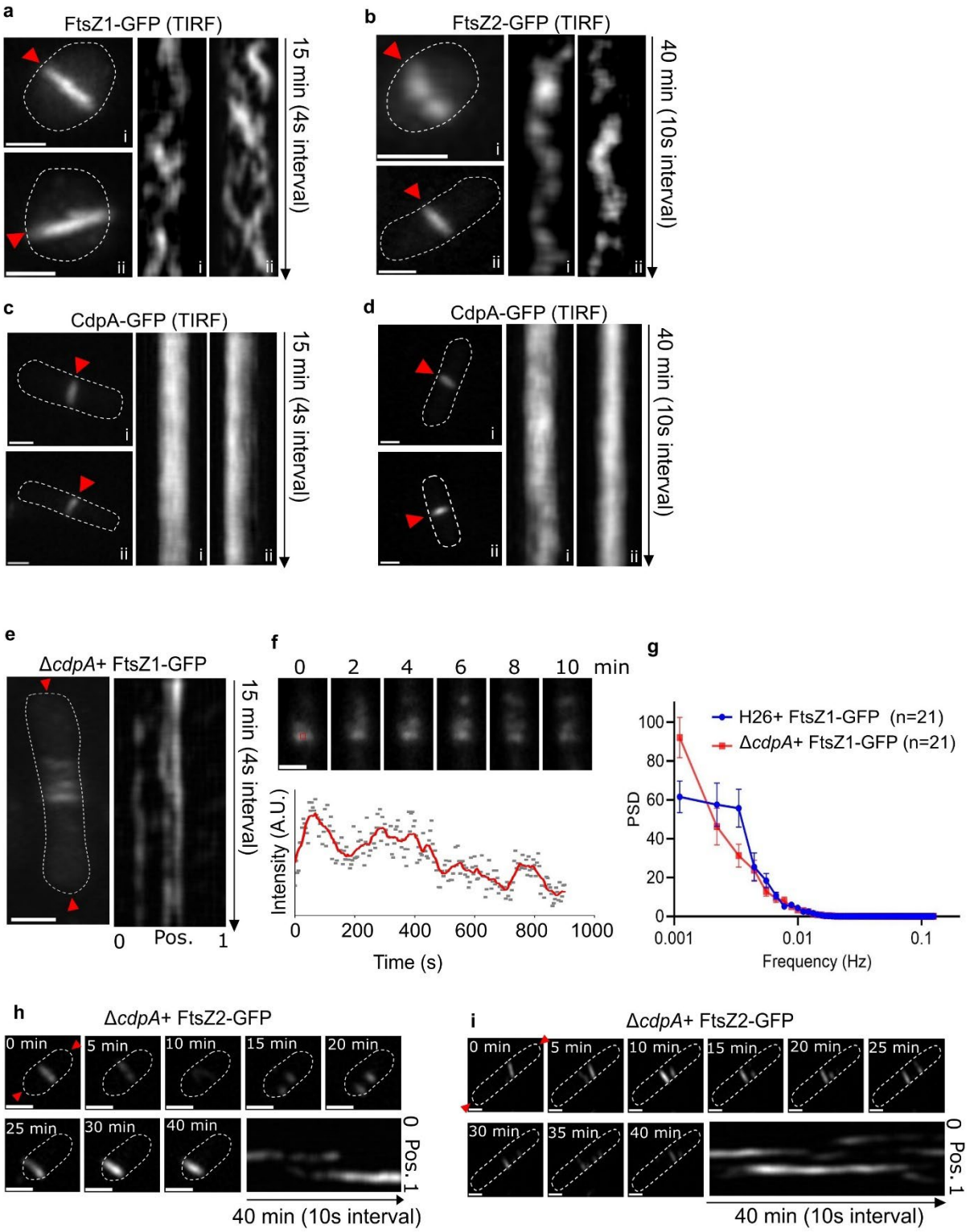

Fig. 4. Division protein localization dynamics and the effect of *cdpA* deletion on FtsZ1 and FtsZ2 movement. Cells were grown in Hv-Cab without tryptophan induction to minimize the expression level of fluorescent fusion proteins. Mid-log cultures were sampled for TRIF imaging. The data shown is representative of at least two independent experiments. **a,** Maximum intensity projections (MIPs) of two representative wild-type H26 cells expressing FtsZ1-GFP (i and ii) are shown on the left, with the corresponding kymographs at positions indicated by red arrows in the MIPs shown on the right. **b,** MIPs of two representative wild-type H26 cells expressing FtsZ2-GFP (i and ii) and their corresponding

920 kymographs. **c-d,** MIPs of wild-type H26 cells expressing CdpA-GFP and their corresponding
921 kymographs with different imaging time-window (4 s intervals for 15 min, panel c; 10 s intervals for
922 40 min, panel d). **e,** MIP of one representative Δ*cdpA* expressing FtsZ1-GFP and its kymograph
923 computed from the intensity along the long axis of cell (between the two red arrows). The relative
924 position (0-1) along the long axis of cell is labelled below the kymograph. **f,** Montages of FtsZ1-GFP
925 dynamics in Δ*cdpA* and the integrated fluorescence time trace for the ROI region, as shown as a small
926 red box around the centre of ring at the start of imaging (Time 0 min). The red curve is the moving
927 average (every 5 points) of the raw intensity (grey dots). Source data are provided as a Source Data
928 file. **g,** The mean power spectral density (PSD) curves (± SEM) of FtsZ1-GFP in wild-type and Δ*cdpA*
929 cells (n=21). Source data are provided as a Source Data file. **h-i,** Montages of representative FtsZ2-GFP
930 dynamics in two Δ*cdpA* cells and their corresponding kymographs indicate the changes in ring position
931 (h) and orientation (i). All scale bars are 1 µm.

932

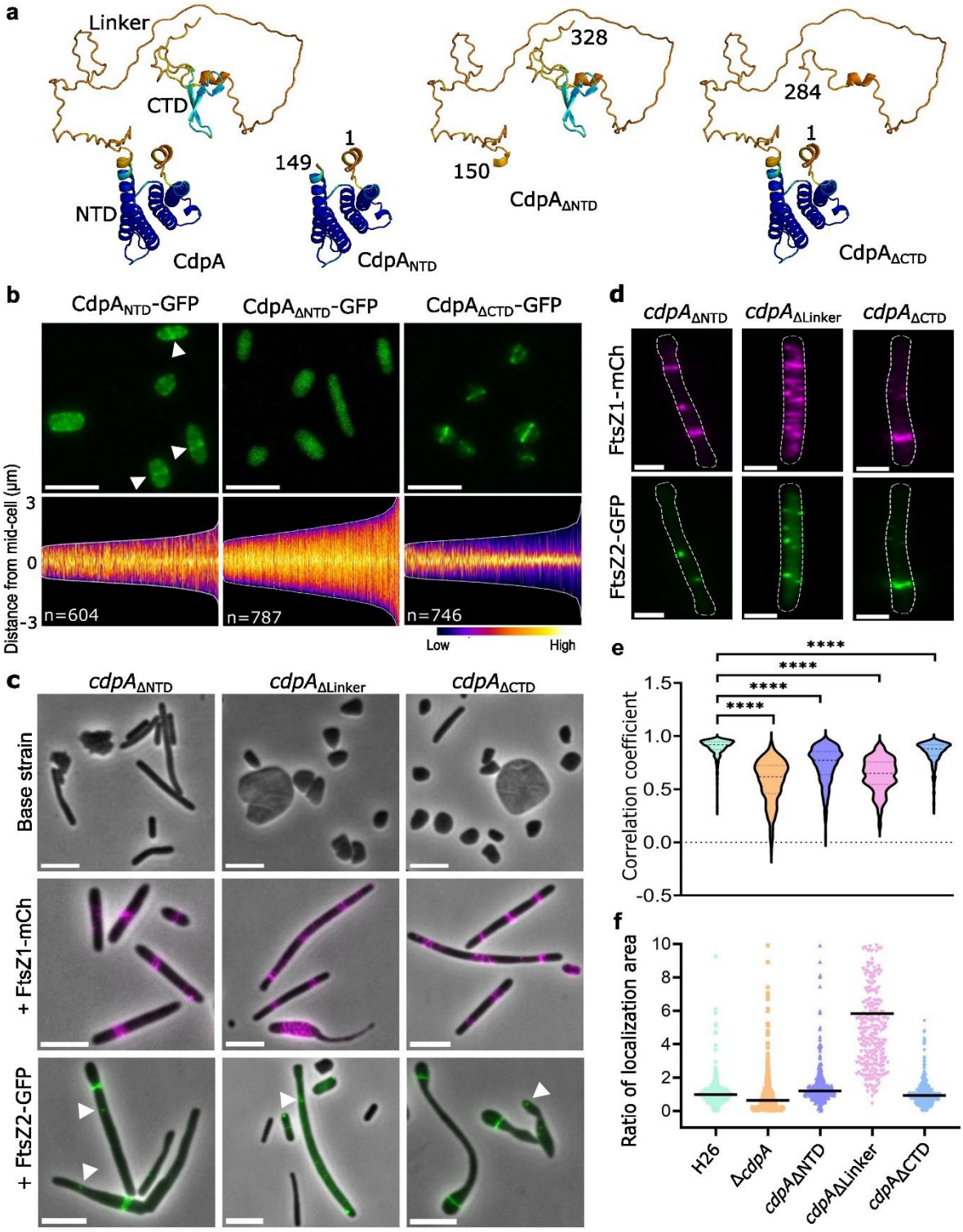

Fig. 5. The three domains of CdpA have different contributions to the role of CdpA in of the organisation of FtsZ1 and FtsZ2. a, Alphafold2 models of CdpA showing domain boundaries of the GFP tagged deletion constructs, including the N-terminal domain (NTD), disordered linker, and C-terminal domain (CTD). **b,** Fluorescence microscopy of H26 wild-type strains expressing the indicated constructs during mid-log growth in Hv-Cab medium with 0.2 mM Trp. Arrows indicate regions of weak mid-cell localization. Scale bars, 5 µm. The lower panels show demographic analyses of fluorescence along the long axis, ordered from shortest to longest cells (left to right). n=number of

941 cells examined over one representative experiment. **c,** Phase-contrast and fluorescence micrographs
942 of the indicated *cdpA* deletion strains producing either FtsZ1-mCherry or FtsZ2-GFP, sampled during
943 mid-log phase growth in Hv-Cab + 0.2 mM Trp. Arrows indicate some faint foci of FtsZ2-GFP. Scale
944 bars, 5 µm. **d,** Fluorescence images of the indicated *cdpA* deletion strains co-producing FtsZ1-
945 mCherry and FtsZ2-GFP. Scale bars, 2 µm. **e,** Distributions of cellular correlation coefficients between
946 FtsZ1-mCherry and FtsZ2-GFP and (**f**) ratio of localization area for FtsZ1-mCherry:FtsZ2-GFP in the
947 background strains shown below the lower panel. The sample sizes analysed for each background
948 strain in panel e were as follows: 587 for H26, 665 for Δ*cdpA*, 397 for $cdpA_{\Delta NTD}$, 424 for $cdpA_{\Delta Linker}$,
949 and 386 for $cdpA_{\Delta CTD.}$ The statistical test in panel e was performed using an unpaired t-test (two-
950 tailed) in Prism, with **** indicating a significant difference (P<0.0001). The sample sizes analyzed
951 for each background strain in panel f were as follows: 471 for H26, 320 for Δ*cdpA*, 349 for $cdpA_{\Delta NTD}$,
952 329 for $cdpA_{\Delta Linker}$, and 447 for $cdpA_{\Delta CTD.}$ For display purpose (with the maximum y-axis set to 10), 112
953 data points fell outside the axis limits. The data shown are representative from one of two
954 independent experiments. Source data are provided as a Source Data file.

955

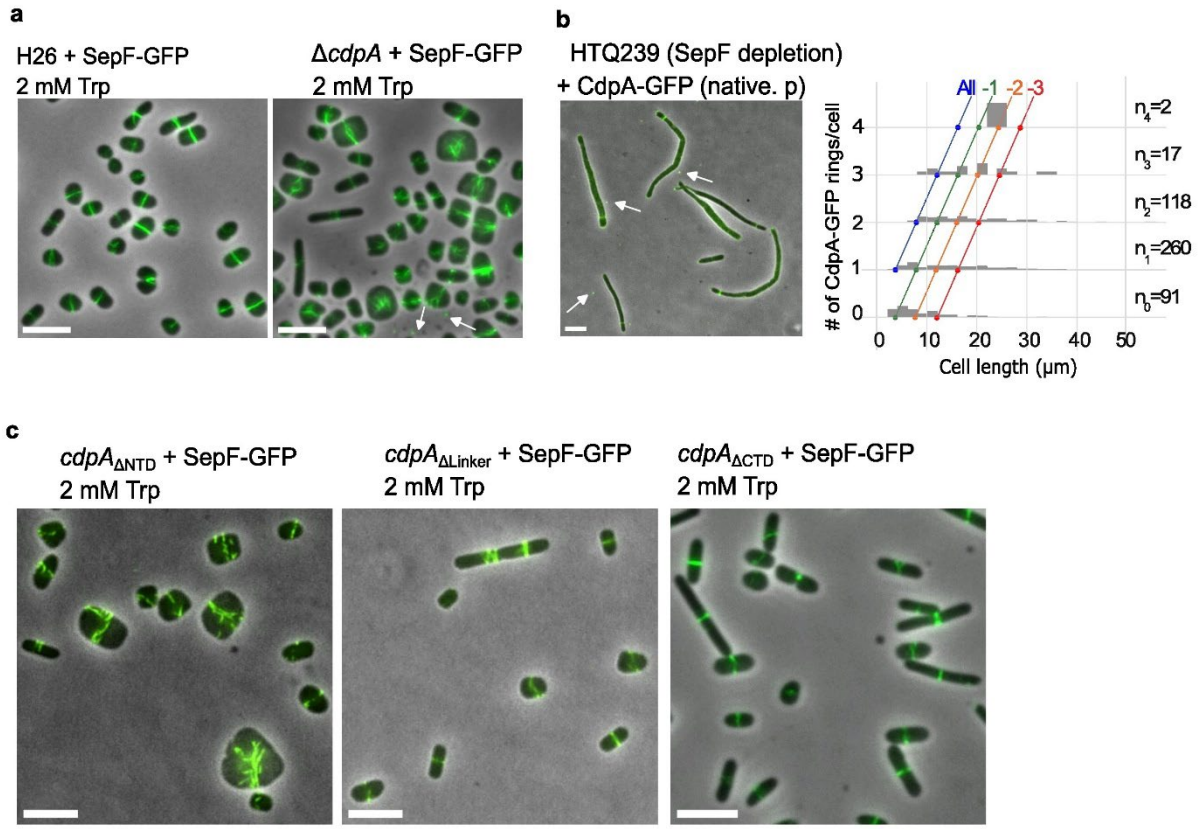

Fig. 6. The interdependency of CdpA and SepF localization. a, Phase-contrast and fluorescence micrographs of wild-type H26 and *cdpA* deletion strains producing SepF-GFP, sampled during mid-log phase growth in Hv-Cab + 2 mM Trp**.** Microscopic images of the strains grown under 0.2 mM Trp can be found in Supplementary Fig. 21. At higher expression levels, SepF-GFP formed branched and less condensed mid-cell bands in the wild-type-like cells in the absence of CdpA. **b,** Phase-contrast and fluorescence micrographs of SepF deletion strain (HTQ239) expressing CdpA-GFP under its native promoter. The histograms show the number (#) of CdpA-GFP rings detected versus cell length. Coloured lines indicate a nominal WT frequency of rings (All), or how many fewer rings were observed, as per Fig. 3c. n= number of cells examined over one biologically independent experiment with indicated ring number, and the data shown is representative of at least two independent experiments. Source data are provided as a Source Data file. **c,** Phase-contrast and fluorescence micrographs of three CdpA domain deletion strains producing SepF-GFP, sampled during mid-log phase growth in Hv-Cab + 2 mM Trp**.** White arrows indicate small extracellular fluorescent particles. All scale bars, 5 µm. The micrographs shown are representative of at least two independent experiments.

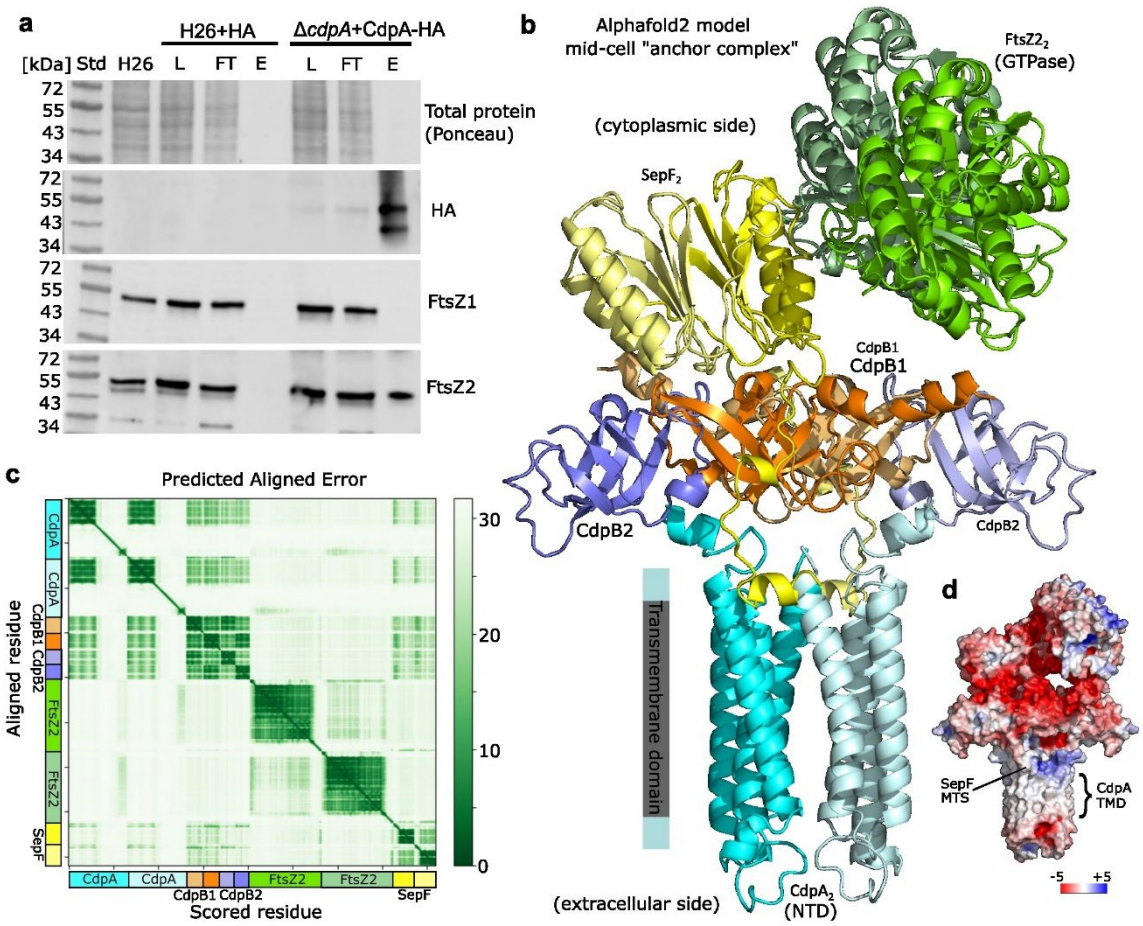

Fig. 7. CdpA is associated with FtsZ2 and other division proteins in a putative membrane anchor complex. a, Western blots of one of three replicate co-immunoprecipitation experiments. The cell lysate (L), unbound protein flow through (FT) and bound protein elution fraction (E) from control (H26 + HA vector only) and Δ*cdpA* + CdpA-HA were analysed by 15% SDS-PAGE and western blotting. The total protein stain (Ponceau S) is shown for the same membrane used for the anti-HA probe, and replicate membranes were probed with anti-FtsZ1 or anti-FtsZ2 as indicated. The control (H26 + HA vector only) was not detectable within the size limits of the gel. **b,** Alphafold2 model of the mid-cell anchor complex generated from a sequence input of 2 CdpA, 2 CdpB1, 2 CdpB2, 2 FtsZ2, and 2 SepF. The C-terminal regions of CdpA and the N- and C-terminal extensions of FtsZ2 that are largely disordered are not shown for clarity. **c,** The Alphafold2 predicted aligned error (%) heatmap plot of all input sequences (concatenated), indicating the degree of confidence in pairwise interactions between residues. **d,** The same structure and orientation as in panel b shown with surface electrostatics, indicating the approximate CdpA transmembrane domain (TMD) and SepF membrane targeting sequence (MTS). Unprocessed western blots and the Alphafold2 coordinates are provided in the Source Data file**.**